JOURNAL OF GEOPHYSICAL RESEARCH, VOL. 100, NO. D12, PAGES 25,877-25,897, DECEMBER 20, 1995

Polar stratospheric clouds and volcanic aerosol during spring 1992 over McMurdo Station, Antarctica: Lidar and particle counter comparisons

A. Adriani,[1] T. Deshler,[2] G. Di Donfrancesco,[3] and G. P. Gobbi[1]

Abstract. Coordinated observations with lidar and balloon-borne particle counters were used to characterize polar stratospheric clouds and to estimate a particle index of refraction. The index of refraction was estimated from comparisons of calculated and measured scattering ratios at a wavelength of 532 nm. The clouds, measured from McMurdo Station, Antarctica (78°S), were observed above 11 km at temperatures below 198 K and were divided into three classes based on their scattering properties and particle size. Clouds with a low scattering ratio, high depolarization, and significant fraction of particles with radii of >2.0 μm had a mean index of refraction of 1.42 ± 0.04 and a mode of 1.43. Clouds with a moderate scattering ratio, low depolarization, and fewer particles of >2.0 μm, had a mean index of refraction of 1.39 ± 0.03 and a mode of 1.37. Ice clouds, apparent from measurements of high scattering ratio, high depolarization, and high concentrations of particles of >1.0 μm, had a mean index of refraction of 1.32 ± 0.02 and a mode of 1.31. Measurements in volcanic aerosol indicated a mean index of 1.43 ± 0.04.

Introduction

Observations of polar stratospheric clouds (PSCs) have been documented for many years [*Stormer*, 1929; *McCormick et al.*, 1982]; however, studies of PSCs have intensified only with the renewed interest in the polar stratosphere following the first evidence of significant ozone depletion there [*Farman et al.*, 1985]. PSC particles are the sites for heterogeneous chemical reactions which free reactive chlorine from its reservoir species and facilitate the removal of reactive nitrogen from the polar stratosphere [e.g., *Solomon*, 1990]. *Crutzen and Arnold* [1986] and *Toon et al.* [1986] first suggested that nitric acid and water (NAW) were the main constituents of PSC particles which formed at temperatures above the frost point. Laboratory measurements then identified nitric acid trihydrate (NAT) as the most probable composition of non-ice PSC particles [*Hanson and Mauersberger*, 1988]. In the Antarctic, field measurements indicated that NO_y is incorporated into PSC particles and that cloud boundaries coincide with saturation with respect to NAT greater than 1.0 [*Fahey et al.*, 1989; *Pueschel et al.*, 1989]. In the Arctic the correspondence between PSC cloud boundaries and saturation with respect to NAT is not so clear. Measurements there often indicate an absence of PSCs in air that is supersaturated with respect to NAT, and significant PSC growth only at quite high supersaturations with respect to NAT [*Rosen et al.*, 1989; *Hofmann et al.*, 1990; *Schlager et al.*, 1990; *Dye et al.*, 1992; *Kawa et al.*, 1992]. These observations of discrepancies between PSC occurrence and the phase boundaries for NAT have led to speculation that PSC particles may be composed of hydrates of HNO_3 other than NAT [*Arnold*, 1992], to additional work investigating the growth of sulfuric acid aerosol due to the uptake of HNO_3 and H_2O [*Worsnop et al.*, 1993; *Zhang et al.*, 1993; *Molina et al.*, 1993], and to new models of PSC particle growth involving condensation of HNO_3 into liquid solution droplets [*Tabazadeh et al.*, 1994; *Drdla et al.*, 1994; *Carslaw et al.*, 1994].

Tolbert [1994] has reviewed three current theories for the formation and growth of PSC particles. The most traditional one involves freezing the stratospheric sulfuric acid aerosol (SSA) and then the nucleation and growth of NAT. The difficulty with this theory is its inability to reproduce the growth of PSC particles observed in field measurements [*Dye et al.*, 1992] and laboratory work indicating that SSA may supercool significantly [*Beyer et al.*, 1994; *Anthony et al.*, 1995]. The second avenue involves the growth of ternary solution drops due to the uptake of H_2O/HNO_3 as temperature cools. When the weight percent of HNO_3 increases above 10%, the droplets crystallize to NAT and further growth proceeds by condensation of H_2O/HNO_3 on the crystalline hydrate [*Molina et al.*, 1993]. The third suggestion does not require the droplets to freeze until the ice point is reached. Instead the droplets may continue to grow as a ternary solution condensing water and nitric acid until the HNO_3 reservoir is virtually depleted [*Tabazadeh et al.*, 1994; *Carslaw et al.*, 1994]. The first two of these theories imply that non-ice PSCs may be predominantly composed of NAT particles, while the third implies a ternary solution droplet.

In the stratosphere all of these growth paths may occur and the dominant particle type is probably controlled by the temperature history, both recent and long-term, of the air parcel. It has been suggested that fast cooling (>5 K day^{-1}) leads to the formation of many small particles which may have an amorphous

[1] Istituto di Fisica dell'Atmosfera, Consiglio Nazionale delle Ricerche, Frascati, Italy.
[2] Department of Atmospheric Science, University of Wyoming, Laramie.
[3] Ente per le Nuove Tecnologie, l'Energia e l'Ambiente, Centro Ricerche Casaccia, S.Maria di Galeria, Italy

Paper number 95JDO2029.
0148-0227/95/95JD-02029$05.00

structure, whereas slow cooling leads to fewer, but larger, particles with perhaps a crystalline structure [*Toon et al.*, 1989; *Hofmann and Deshler*, 1989; *Poole et al.*, 1990; *Schlager et al.*, 1990]. The long-term history of the air parcel may be important in determining the phase of the particles on which PSCs initially nucleate and grow [*Larsen et al.*, 1995; *Tabazadeh et al.*, 1995]. In the Antarctic, where the vortex is more stable and temperatures are colder, much of the vortex stratosphere probably remains below the melting temperature (210 K) of SSA [*Middlebrook et al.*, 1993] for most of the winter and early spring. Thus SSA in the vortex which had been frozen would remain so. The temperature at which SSA droplets freeze, however, is not well known. *Jensen et al.* [1991] suggest that the phase change occurs when the SSA reaches the ice point, but other calculations [*Luo et al.*, 1994] and laboratory work [*Gable et al.*, 1950; *Middlebrook et al.*, 1993; *Anthony et al.*, 1995] indicate that SSA may significantly supercool. In the Arctic stratosphere, where temperatures are warmer and the vortex less stable, there is a higher probability that air masses leading to PSC formation had experienced recent temperatures above the melting temperatures of SSA [*Larsen et al.*, 1995; *Tabazadeh et al.*, 1995], thus contributing to the possibility that Arctic PSCs have more variety than their southern counterparts.

The initial lidar measurements of PSCs separated the observations into two classes, one with high scattering ratio (SR) and high depolarization and the second with moderate SR and low depolarization [*Poole and McCormick*, 1988; *Kent et al.*, 1990]. On the basis of the temperatures at which clouds with these characteristics were observed the first category is associated with ice PSCs, and the second with non-ice PSCs. The non-ice PSCs were observed at temperatures within 5 K of the frost point, and these particles have been assumed to be NAT. Lidar measurements in 1989 indicated that the non-ice PSCs could be further divided into two subclasses [*Browell et al.*, 1990]. The more common observations were in clouds with moderate SR and low depolarization typical of previous observations in non-ice PSCs. The second category of non-ice PSCs was in clouds which gave a low SR but high depolarization. Additional lidar measurements since these initial ones further support the notion that non-ice PSCs can be divided into two categories along these lines [*Rosen et al.*, 1993; *Schäfer et al.*, 1994; *Godin et al.*, 1994]. From an analysis of *Browell et al.*'s [1990] measurements and back trajectory calculations, *Toon et al.* [1990] concluded that PSCs with moderate SR and low depolarization were composed of spherical particles with radii near 0.5 μm and had experienced cooling rates in excess of 5 K day^{-1}, while the PSCs exhibiting low SR and high depolarization contained nonspherical particles with volume equivalent radii of 1.0 μm and had experienced cooling rates considerably less than 5 K day^{-1}.

Laboratory measurements of the condensation of HNO_3 and H_2O on thin films have indicated that NAT is the most likely crystalline form [*Hanson and Mauersberger*, 1988; *Middlebrook et al.*, 1993; *Iraci et al.*, 1994], while *Worsnop et al*, [1993] indicated that the metastable dihydrate may form as a precursor to NAT. Other laboratory work, using vapor ratios of HNO_3/H_2O more representative of stratospheric conditions, suggests that PSCs may have HNO_3/H_2O compositions closer to a penta- or higher hydrate of HNO_3 [*Marti and Mauersberger*, 1993]. *Zhang et al.* [1993] and *Molina et al.* [1993], investigating the behavior of cooled solutions of $H_2SO_4/HNO_3/H_2O$ show that the ternary solution may exist down to temperatures approaching the ice point.

Relating laboratory work to field measurements is possible if the optical character of these various forms of NAW are different. *Deshler et al.* [1991] and *Adriani et al.* [1992] compared lidar and in situ measurements in PSCs to infer the PSC index of refraction (m) which was compared with theoretical values. Recent laboratory measurements of m for various compositions of PSC-like films provide a firmer basis for this technique. *Koehler et al.* [1992], *Berland et al.* [1994], and *Middlebrook et al.* [1994] have made such measurements on thin amorphous and crystalline HNO_3/H_2O films. *Koehler et al.* [1992] found two forms of NAT, although only one appears stable at stratospheric temperatures. Both *Berland et al.* [1994] and *Middlebrook et al.* [1994] measured m for these various HNO_3/H_2O films at a wavelength of 632 nm. They found for amorphous HNO_3/H_2O that m increases from 1.35 to an asymptotic value of 1.47 as the mole fraction of HNO_3 increases from 0.1 to 0.5. For the hydrates of HNO_3 the pattern was similar with m increasing from 1.46 to >1.5 as the mole fraction of HNO_3 increased from the trihydrate to monohydrate.

The purpose of this paper is to compare near-simultaneous measurements of PSCs, using lidar and balloon-borne optical particle counters. The lidar measurements characterize the SR and depolarization properties of the aerosol, and the particle counters their size and number density. Phase, shape, and composition determine particle index of refraction which, along with size distribution, controls the scattered radiation observed from these particles. If the particles are nonspherical or crystalline, they will depolarize backscattered light. Ideally, if the size distribution and scattered radiation of an ensemble of particles are known, then the particle index of refraction can be inferred. This approach has been used in previous years to compare measurements in PSCs [*Adriani et al.*, 1992], in background stratospheric aerosol [*Deshler et al.*, 1991], and in fresh volcanic aerosol [*Deshler et al.*, 1992]. The number of observations in PSCs during these two years, however, was not nearly as extensive as the number of observations in 1992 at McMurdo Station, Antarctica (78°S), which form the subject of this paper.

Instrumentation and Methodology

During the 1992 late winter and early spring, seven concurrent measurements with ground-based lidar and balloon-borne particle counters were performed at McMurdo Station (78°S, 167°E), Antarctica. These measurements were completed on August 27, 29, and 31, September 9 (2 sets) and 14, and October 9, in a variety of stratospheric temperature conditions. PSCs, both non-ice and ice, and volcanic aerosol were observed. Besides these measurements the lidar performed measurements on a daily basis during the period August 26 to October 10. The results of ozone profiles measured at McMurdo during this period are reported by *Johnson et al.* [1994].

The lidar has been operating at McMurdo since 1990, and

the present system configuration has been described by *Adriani et al.* [1992]. The lidar measures the total atmospheric backscattering and depolarization at 532 nm. The backscattered signal arises from scattering by both molecules and aerosol. To assess only the contribution from aerosol particles, we use scattering ratio, the ratio of the scattering measured to the scattering expected from a purely molecular atmosphere. The molecular backscattering is normalized to 1 after the lidar signal is calibrated with a molecular density profile inferred from temperature and pressure soundings. SR then gives a vertical profile of the atmospheric particle content, with a vertical resolution as fine as 150 m. From atmospheric molecular density profiles, the volume particle backscattering cross section can be retrieved. Although this is more directly comparable to particle measurements, SR is adopted because it is more sensitive to small features at the upper levels.

Depolarization, given in percentage, is a measure of the degree of depolarization of the backscattered light from an incident polarized laser beam. It is the ratio of the depolarized signal to the undepolarized signal. Spherical particles do not cause depolarization, and thus a depolarized signal indicates the presence of aspherical, i.e., solid, or mixed solid/liquid particles. High depolarization ratios can be correlated to crystalline particle structure. The depolarization due to air molecules is about 1.4% at 532 nm [*Young*, 1980].

Balloon-borne optical particle counters (OPCs) have been used to study PSCs in Antarctica since 1987 [*Hofmann et al.*, 1989; *Hofmann and Deshler*, 1991; *Deshler et al.*, 1991; 1994]. They provide in situ observations of integral number densities. The instruments were improved in 1989 such that since then particles with radii larger than 0.15, 0.25, 0.5, 1, 2, 3, 5, and 10 μm can be measured. Bimodal lognormal distributions are found to represent the measured size distributions in most cases. To obtain the total number concentration of aerosols, separate balloon-borne measurements of condensation nuclei (CN) were conducted periodically during the time interval. In 1992, CN profiles were measured on August 24, September 9, and September 23. For use with the measurements of aerosol 0.15 to 10.0 μm, the CN measurement closest in time to the OPC measurement was used. As shown by *Deshler et al.* [1994], the CN concentrations between 10 and 25 km were very consistent from sounding to sounding with values between 8 and 20 cm^{-3}. Example size distributions and comparisons with measurements from the OPCs have been given [*Hofmann and Deshler*, 1991; *Deshler et al.*, 1993; *Deshler*, 1994]. Discussions of the effect of statistical errors in the OPC measurements are given by *Deshler et al.* [1993] and below. Once the aerosol size distribution has been determined, the backscattering expected at the wavelength of the lidar, 532 nm, can be calculated along with aerosol surface areas and volumes, assuming that the particles are spherical.

For each of the seven measurement pairs completed with both lidar and particle counters the measurements are assumed to be completed in the same air mass. In reality, the measurements are separated by up to 120 km, since the lidar is ground-based and the particle counter moves with the wind. Wind speed measurements from meteorological soundings at McMurdo were used to estimate an appropriate temporal sequence from the lidar profiles to compare with a balloon-borne instrument drifting with the wind. The validity of this assumption will be reduced during certain situations, such as the propagation into the stratosphere of gravity waves generated downwind of the Transantarctic Mountains. In these cases, localized formation of ice clouds has been observed, and characteristics of particle size and number density can vary significantly over a range of few tens of kilometers [*Adriani et al.*, 1992].

Observations

The lidar and aerosol measurements completed in 1992 at McMurdo have been separately described by *Gobbi and Adriani* [1993] and *Deshler et al.* [1994]. Here we present a comparison of these two data sets. Figure 1 describes the measurements taken on August 29, 1992. Starting from the left, the three panels depict the aerosol particle mixing ratio at several sizes, the lidar SR and depolarization, and temperature. The particle counter measurements are reported as profiles of integral mixing ratios of particles with radius larger than the value indicated. The short-dashed lines present measurements completed on October 9 when McMurdo was under the edge of the polar vortex. The October 9 measurement is used to represent the polar vortex stratospheric aerosol when temperatures were too warm for PSC formation during the spring of 1992. It is indicative of the volcanic aerosol cloud just before the vortex breakup and is assumed to be indicative of the particulate matter in the vortex on which PSCs formed during the colder season. To compare vertical aerosol profiles, the October 9 profiles are shifted upward by 1.2 km. The criterion used in shifting this profile consisted of making the volcanic aerosol cloud SR at the base of the stratosphere, between 9.5 and 11 km, coincide with the lidar profile observed on August 29. This displacement is mainly expected due to the lifting of isentropic surfaces in the inner vortex compared to the vortex margins [*Shoeberl et al.*, 1992] and was confirmed by observations of a general descent of the volcanic aerosol close to the polar vortex border [*Gobbi and Adriani*, 1993]. The vertical position of the aerosol cloud is quite conservative with respect to isentropic surfaces. Thus the relative displacement of the cloud in the vertical may give an indication of the position of the vortex center with respect to McMurdo. On October 9 the vortex border was roughly above the station.

To provide a functional form for the size distributions measured by the OPC, lognormal size distributions are used. For measurements in PSCs this usually requires bimodal distributions. Each lognormal distribution is specified by three parameters: the total number concentration, N_i; the median radius, r_i; and the distribution width, σ_i. The values for the distribution parameters are selected to minimize the difference between the calculated and measured number concentration for each size channel. The uncertainty in the aerosol concentrations measured increases as the number of particles measured decreases owing to counting statistics. The impact of this uncertainty on the lognormal parameters and the derived surface area and mass was estimated by using a Monte Carlo simulation to vary the aerosol concentrations within their uncertainty limits and refitting size distributions. The result was an average variation of 10-20%, with a maximum variation of 30-40%, for surface area and mass

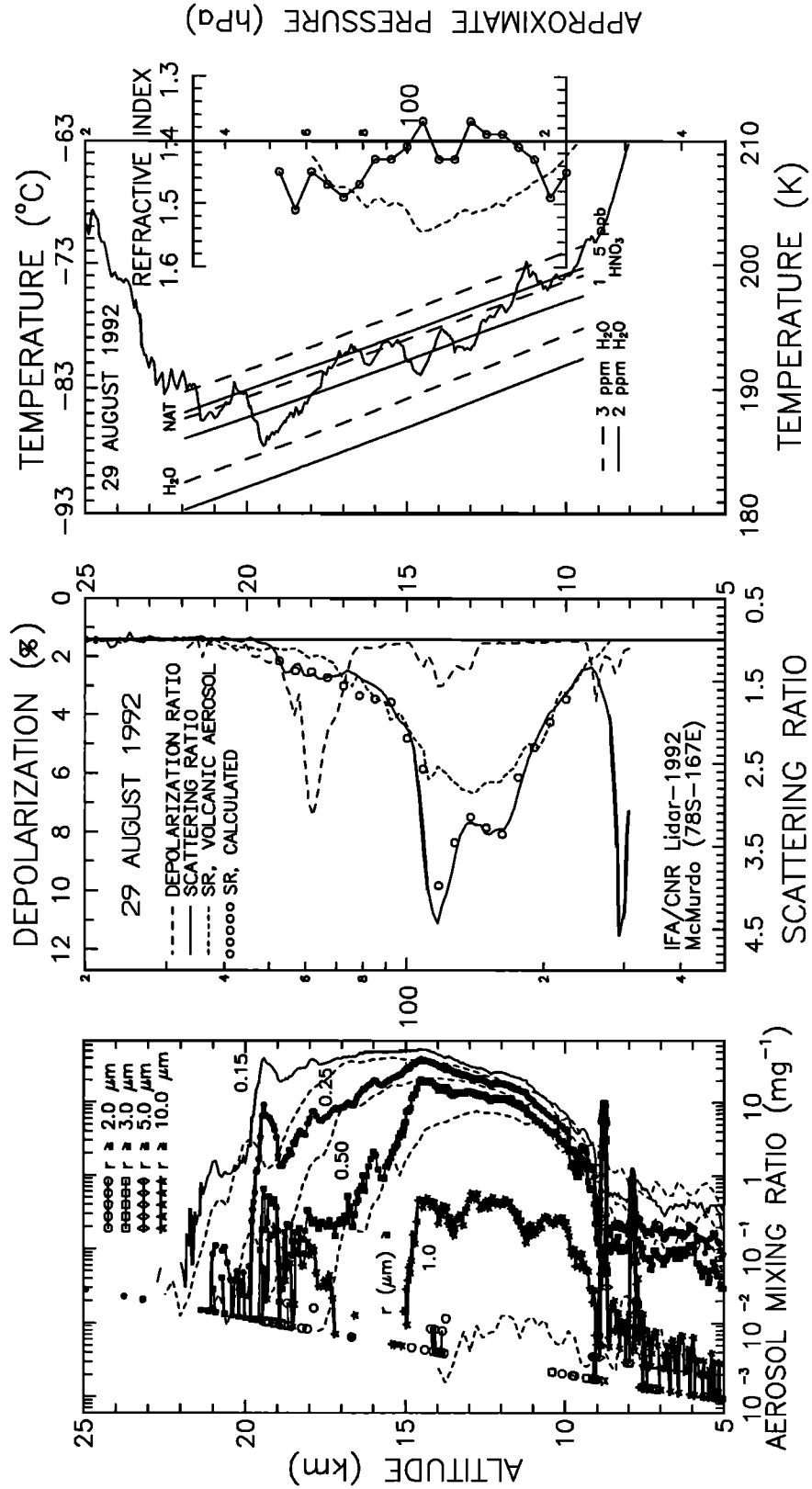

Figure 1. Comparison of the particle counter and lidar measurements completed on August 29, 1992. (Left) Mixing ratios of particles larger than 0.15, 0.25, 0.5, 1, 2, 3, 5, and 10 μm, measured by particle counter. (Center) SR and depolarization measured by lidar at 532 nm. The calculated SR is also shown (open circles). The vertical line starting from 1 on the SR axis and 1.4 on the depolarization axis provides the molecular atmosphere references. (Right) Temperature profiles measured on the particle counter flight, equilibrium temperatures for NAT and water ice at various vapor mixing ratios, and estimated particle index of refraction. The equilibrium existence temperatures are for 2 and 3 ppmv H_2O and 1 and 5 ppbv HNO_3. The short-dashed lines in each panel represent the aerosol mixing ratios, SR, and temperature measured on October 9, 1992, when temperatures were too warm for PSC formation. The October 9 measurements have been increased in altitude by 1.2 km as discussed in the text.

concentrations and for σ_1, r_2, and σ_2. Variations in r_1 and N_2 were as high as a factor of 2 for small values of these quantities. N_1 is measured with the CN counter and has an uncertainty of <3% for concentrations near 10 cm^{-3}. With the use of the derived size distributions the SR was calculated by integrating, over the size distribution, the backscattering expected from each particle size. The error on the measured SR is low. At an altitude of 15 km we estimate an error of <1% for SR ≈ 2.

The rightmost curve on the third panel in Figure 1 is an estimate of the refractive index of the particles. The refractive indices reported provide the best match of the SR calculated, from the measured aerosol size distributions, with the SR measured by lidar. Depending on vertical structure, averages over 150-500 m were used for the profile comparisons. The real part of the index of refraction was allowed to vary in the range 1.31-1.60, using steps of 0.02. At each step (each value of m) the sizes measured by the OPC were calculated on the basis of the response of the OPC for that value of m. These sizes and their associated number concentrations were used to determine the optimum values of the parameters of the bimodal/unimodal lognormal size distributions. The SR was then calculated on the basis of Mie theory and compared to the measured SR. The optimum m was obtained by minimizing $|SR_{calc} - SR_{meas} + 10(m_{assumed} - m_{inferred})|$. Thus the comparison is weighted to force the assumed and inferred index of refraction to be close. At a forward scattering angle of 40° the response of the OPC is monotonic with particle size over the range of m considered [*Hofmann and Deshler*, 1991]. The imaginary, or absorptive, component of m is assumed to be zero. From the Monte Carlo simulation above the uncertainties in m, based on uncertainties associated with the OPC measurements, were found to be of the order of 0.01 to 0.02.

Since Figure 1 illustrates the basic measurements and their comparison, a few additional points are worth illustrating. Between 11 and 15 km, particle concentrations were increased above the volcanic aerosol level mainly for particles of ≥0.5-μm radii. A small depolarization was also observed around 14 km, in correspondence with low concentrations of particles >2-μm radii. In the complete set of measurements an increase in depolarization was observed whenever particles >2 μm were present. The wave-like structure in the temperature profile, probably due to the propagation of lee waves generated downwind of the Transantarctic Mountains, does not seem to introduce large discrepancies between the OPC and lidar measurements. In the 14- to 15- and 17- to 20-km region, changes in the lidar signal correspond to changes in the size of the particles measured, and the maximum depolarization between 17 and 19 km coincides with the presence of larger particles. Slight discrepancies in altitude can be attributed to the presence of the wave-like structure in the atmosphere and the different location of the lidar and aerosol counter. Above 20 km the number of particles decays rapidly, and the lidar signal diminishes as well.

Figure 2 presents 20 lidar profiles spanning the period August 26 to October 9. The dotted line repeated in each panel is the 9 October profile adjusted for altitude as described earlier. The magnitude of the displacement of the October 9 profile is indicated on each panel. On one occasion, September 11 (920911 on Figure 2), a displacement in altitude of 2.4 km was observed, although typically the displacements were 1.5 km or less. The relatively constant Δz of 1.0-1.5 km indicates that the region of the vortex sampled was relatively homogeneous. Comparison of each lidar profile with October 9, gives an indication of PSC activity (e.g., 920826, 920830, 920909) and days when there were only minor, or no, deviations from the volcanic profile (e.g. 920827, 920918). Included in Figure 2 are all PSC events observed over McMurdo in spring 1992 by lidar. As has already been mentioned, the characteristics of PSCs depend not only on the temperature at the time of the observation, but also on the history of the air parcel. This is particularly true for non-ice clouds. Trajectory analysis of the PSC air masses showed that in some cases they reached latitudes about 60°-70°S before moving southward [*Gobbi and Adriani*, 1993] and that the air coming from the lower latitudes was often lifted and cooled. The solid circles indicate altitudes at which trajectory analyses were performed. The results of this analysis will be presented later.

From comparisons similar to Figure 1, and roughly summarized in Figure 2 for the six sets of measurements, the clouds observed were classified into four categories: volcanic aerosol, nondepolarizing hydrated nitric acid particles (NAWn), depolarizing hydrated nitric acid particles (NAWd), and ice. Volcanic aerosol measurements can be identified, since they do not differ significantly from the altitude-adjusted October 9 profile (see Figure 2). In regions where the particle measurements (both lidar and particle counter) differ from the volcanic profile, regions of moderate SR and low depolarization are classified as NAWn, those of low SR and high depolarization as NAWd, and those of high SR and high depolarization as ice. The basic criteria for three of the classes are illustrated in Figure 1. Between 9.5 and 11 km and 15 and 16.5 km the coincidence of the profile on August 29 with the volcanic profile on October 9 marks the volcanic aerosol. The cloud containing the increased aerosol concentration in the interval 11-15 km is classified as NAWn, i.e., moderate SR and low depolarization. Between 17 and 19 km, where lower SRs and higher depolarizations are observed, the particles are classified as NAWd. The fourth category, not represented here except perhaps briefly at 19.5 km, is associated with ice clouds. The observation of two distinct scattering and depolarization signals from non-ice PSCs was first made by *Browell et al.*, [1990]. Our classification of particles and measurement of particle size are in general agreement with Browell et al.'s measurements and *Toon et al.*'s [1990] conclusions.

Based on comparisons similar to Figure 1 for the other days when measurements were completed, a data set of estimated particle index of refraction was generated and subdivided into the four classes defined. The set of measurements was limited to exclude those cases in which confidence in the inferred value of m was low. Only cases when the SR was greater than 1.14 were considered. We also required that changes in m produce significant changes in the calculated SR. Cases in which the calculated SR was relatively insensitive to changes in m were excluded. Recall that m is inferred from a comparison of calculated and measured SR. The spread of the calculated SR normalized to the average calculated SR is plotted in Figure 3. In the data set for analysis, cases in which the range of calculated SR was <40% of the average SR were excluded.

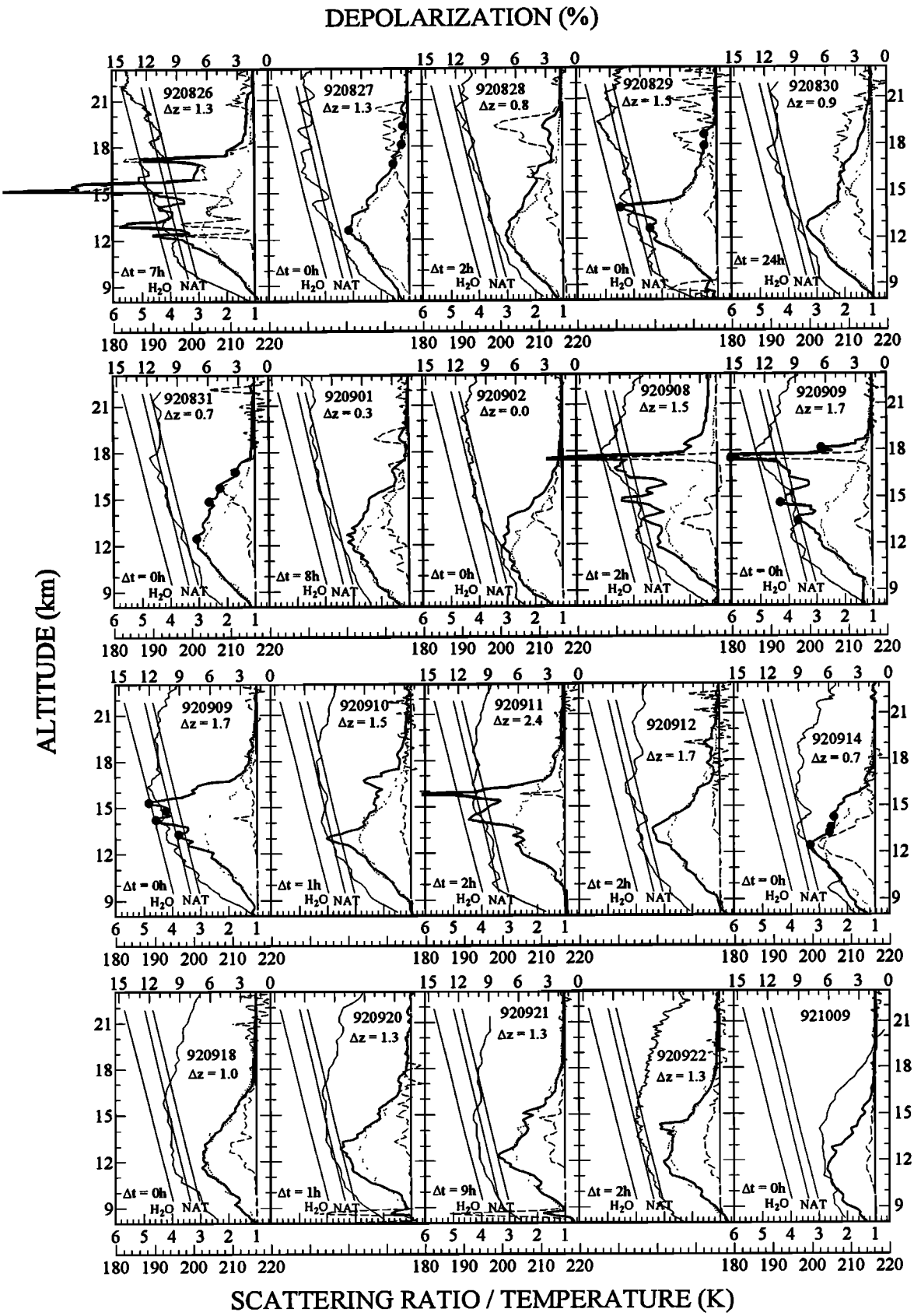

Figure 2. Profiles of SR, depolarization, and temperature measured at McMurdo between August 26 and October 9, 1992. The repeated SR (dashed line) shown in each figure represents the October 9 measurements. The altitude (Δz) by which the October 9 profile is adjusted in each profile is indicated on that panel. Equilibrium existence temperatures for water ice and NAT are also shown, assuming 3 ppmv H_2O and 1 and 5 ppbv HNO_3. Here Δt is the time difference existing between the lidar and temperature balloon sounding. The solid circles on the SR curve mark the level where back trajectories were computed.

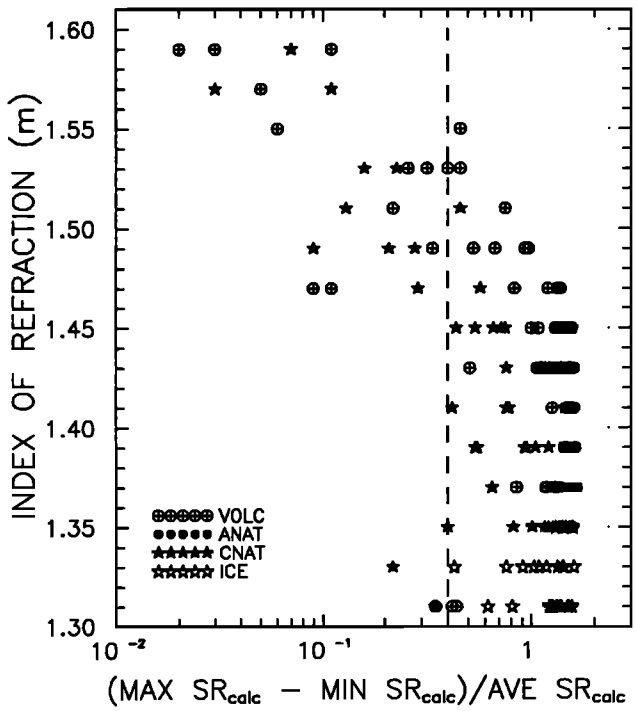

Figure 3. Estimated index of refraction as a function of the ratio of the range of computed SR normalized to the center point of the SR range. See text for further explanation.

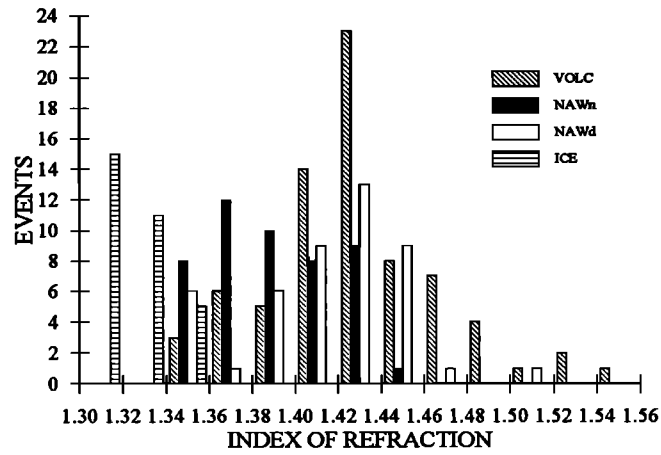

Figure 4. Histogram of the computed indices of refraction for each category: non depolarizing hydrated nitric acid (NAWn), depolarizing hydrated nitric acid (NAWd), ice, and volcanic aerosol (VOLC).

For the non-ice aerosol the best value of m was found well away from the boundaries of the range over which m was varied, except for two cases, suggesting that the range of m considered was not unrealistically restricted. For the cases classified as ice, 15 of these layers resulted in a value of m = 1.31, the lower boundary of the range considered. Of these 15, 10 displayed a good agreement between calculated and measured SR. The other five cases all occurred during the first measurement set on September 9, 1992, and the calculated SR was a factor of 2-10 higher than the measured SR. Thus the inferred m could have ranged significantly below 1.31. These discrepancies resulted, we believe, from a poor correspondence of the altitudes of the layers measured by the two instruments. On this day there were quite thin aerosol layers particularly those layers with ice characteristics.

The index of refraction histograms in Figure 4 represent 199 measurements classified according to the above criteria. The index of refraction distribution for volcanic aerosol is roughly Gaussian with a mode at 1.43. The distribution for NAWn has a mode at 1.37, skewed to higher m, while NAWd has a mode at 1.43 skewed to lower m. Ice has a mode at 1.31. The average values of m and their standard deviations are: 1.43 ± 0.04 for volcanic aerosol, 1.39 ± 0.03 for NAWn, 1.42 ± 0.04 for NAWd, and 1.32 ± 0.01 for ice. The general characteristics of the distributions are also described in Table 1.

On the basis of the depolarization and size measurements it is clear that in PSCs containing NAWd some of the particles are nonspherical. We did not attempt to model scattering from aspherical particles because of the difficulties involved and because we have no a priori information concerning particle shape. On the basis of the agreement of m, calculated for those polar stratospheric clouds which could be clearly indentified as ice clouds, with that expected for ice, even though these particles were also assumed to be spherical, indicates that this distinction may not cause significant changes in our estimates of m.

Laboratory measurements of the index of refraction for thin crystalline and amorphous HNO_3/H_2O films give values of 1.43, 1.45, and 1.47 for amorphous NAW at stoichiometric ratios corresponding to the trihydrate, dihydrate, and monohydrate [*Berland et al.* 1994]. For crystalline dihydrate and monohydrate

Table 1. Characteristics of Particles in the Categories NAWn, NAWd, ICE, and VOLC

	NAWn [50]	NAWd [46]	ICE [29]	VOLC [74]
Concentration, cm^{-3}	9.4-23	5.7-31	6.7-12	6.7-91
Surface area, $\mu m^2\ cm^{-3}$	19-50	1-32	4.7-126	3.8-44
Volume, $\mu m^3\ cm^{-3}$	3.3-15	0.2-5.4	0.5-86	0.3-8.6
Index of refraction	1.39 ± 0.03	1.42 ± 0.04	1.32 ± 0.01	1.43 ± 0.04
Scattering ratio	2.5-4.9	1.1-3.1	1.1-8.7	1.1-3.2
Depolarization	1.5-3.7	2.3-6.9	1.4-19	1.4-2.4
Concentration > 2.0 μm, mg^{-1}	<0.006	0.001-0.06	0.01-9.0	<0.01

VOLC is volcanic aerosol. The number of points considered in the statistics are shown in the square brackets.

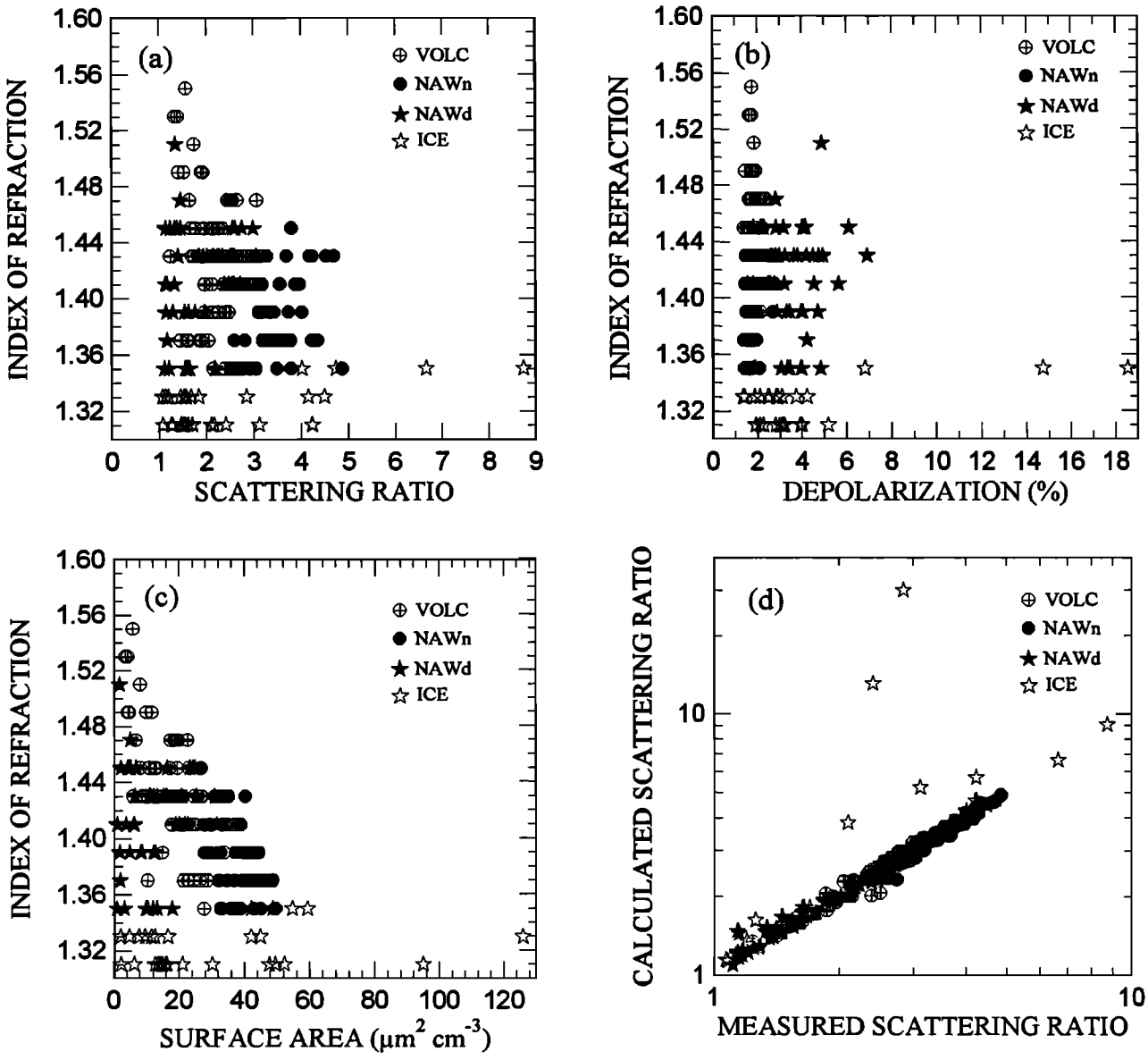

Figure 5. Index of refraction as a function of (a) measured SR, (b) depolarization, (c) computed surface area densities from the particle counter measurements, and (d) Computed SR versus measured SR. Measurements are grouped into the four categories.

they measured 1.51 and 1.54 with errors of the order of ±0.01 but were unsuccessful in growing crystalline NAT. These measurements were performed at a wavelength of 632 nm and at temperatures lower than 175 K. Later, *Middlebrook et al.* [1994] repeated these measurements on thin nitric acid/ice films, using a slightly different technique, and obtained results similar to those of Berland et al. for amorphous NAW and for crystalline monohydrate. They were also successful in growing crystalline NAT; however, the NAT was not stable during the measurement sequence. Refractive indices measured for NAT decreased from 1.46 to 1.42. The cause of this change is not well known, although it is suggested to be the result of changes in the optical scattering due to inhomogeneities in the film. Our results at 532 nm, 1.39 ± 0.03 for NAWn and 1.42 ± 0.04 for NAWd, are consistent with the laboratory results for an amorphous particle with stoichiometry similar to a tri- or higher hydrate, or with the lower range of Middlebrook et al.'s measurements on crystalline NAT. It is not known whether crystalline NAT particles in the atmosphere would age like the samples in the laboratory.

In Figure 5, scatterplots of index of refraction versus SR, depolarization, and surface area for the four measurement categories are shown. SR and depolarization are directly measured by lidar. Particle surface area is calculated from the particle size distributions. The four aerosol categories assume well-defined locations in the scatterplots according to their main characteristics. In all the comparative measurements, SR was never larger than 9, and depolarization never larger than 19%. In other lidar measurements, in a well-developed ice cloud, SRs larger than 12 and depolarizations close to 50% were observed, but in situ measurements were not made at these times. In the ice cloud

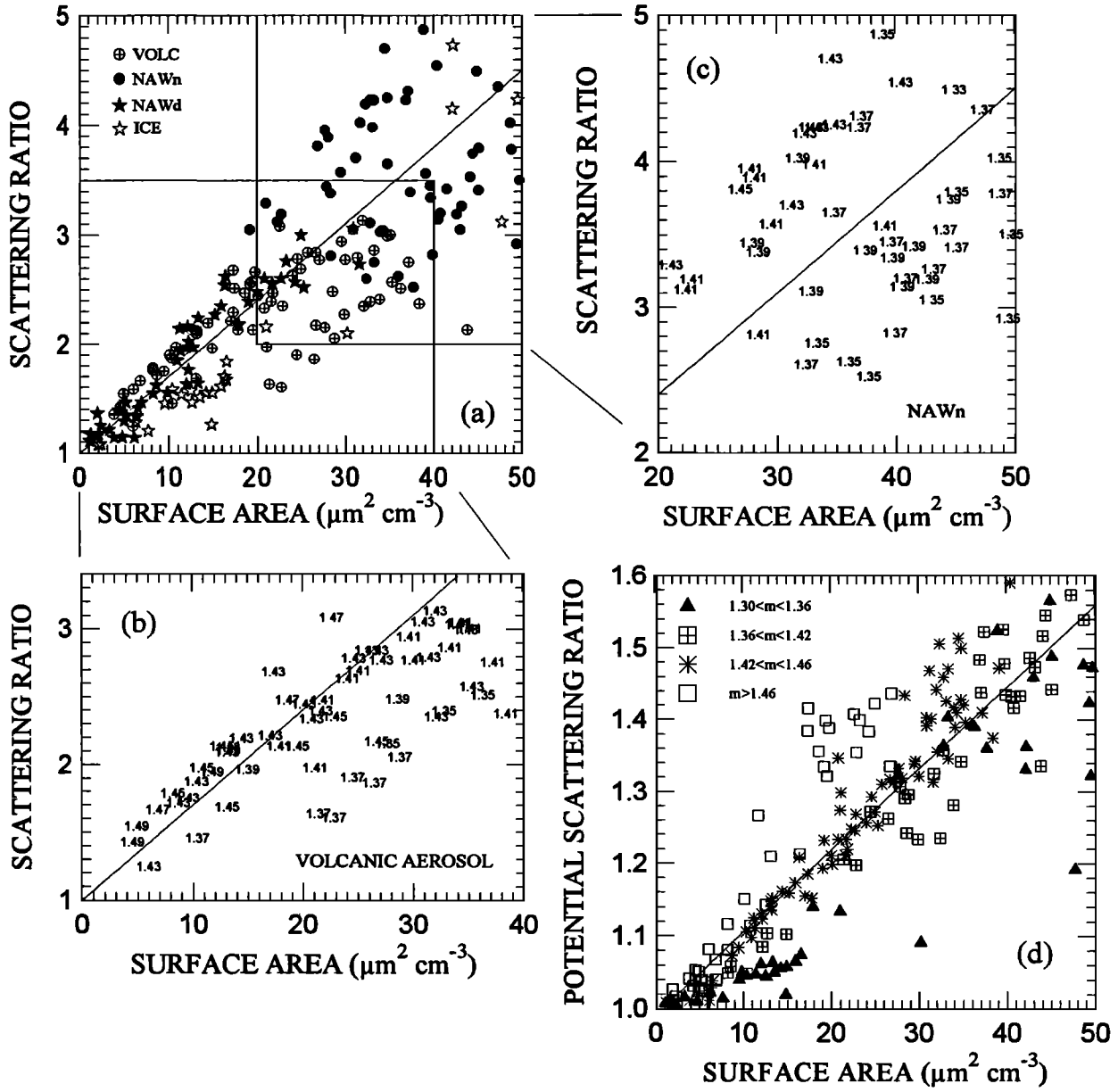

Figure 6. Relationship between SR and surface area (a) For all the comparison measurements divided into the four categories. The linear dependence is shown with the best fit line to the data and for reference is repeated in Figures 6b, 6c, and 6d. (b) Same as Figure 6a except for only the volcanic aerosol with the individual values of *m* listed on the plot. (c) Same as Figure 6b except for NAWn. (d) Same as Figure 6a except the comparison measurements are grouped by the range of estimated *m*.

category all cases are included in which the calculated index of refraction was around the ice value of 1.31. Low values of SR and depolarization are assumed to represent the first stage of evolution, or measurements near the top or bottom, of these clouds.

A general increase of the area of the particles is observed for decreasing refractive index. This point is consistent with the fact that the particles grow mainly by condensing water on their surfaces. As volcanic aerosols cool, they grow initially through deliquescence [*Steele and Hamill,* 1981] and then through the cocondensation of HNO_3 and H_2O. Although the ratio of nitric acid to water for crystalline hydrates in the atmosphere is often assumed to be 1:3 [*Hanson and Mauersberger,* 1988], other work points to the importance of lower hydrates [*Worsnop et al.,* 1993], higher hydrates [*Marti and Mauersberger,* 1993], and ternary liquid solutions [*Carslaw et al.,* 1994]. In any case, as the particles grow either through deliquescence or cocondensation of HNO_3 and H_2O, *m* is likely to decrease owing to the uptake of water.

The relationship between SR and surface area is shown in Figure 6a, which includes the points with surface area densities of <50 μm^2 cm^{-3}. The average linear dependence of surface area on SR is shown by the fitted line. Figures 6b and 6c present additional details of Figure 6a for the categories of volcanic aerosol

and NAWn, respectively. The value of m calculated for each point in these categories is shown along with the fit line from Figure 6a. Comparison of the indices of refraction of volcanic aerosol and NAWn in Figure 6b and 6c with the fit line indicates that the points to the right contain more water. The index of refraction is generally lower on this side, approaching values near 1.35, a result already illustrated in Figure 5c. SR and surface area do not show the same dependence with decreasing index of refraction. For a constant SR in Figures 6b and 6c, as surface area increases, m decreases.

To eliminate the dependence of SR on altitude, due to the decreasing molecular density, surface area is plotted against potential scattering ratio (PotSR) in Figure 6d. PotSR is the SR that would be measured if the scattering particles were moved to the surface, and it is calculated by using

$$\text{PotSR} = \frac{T_0 p}{p_0 T} (\text{SR} - 1) + 1.$$

T and p are the temperature and pressure at the measurement altitude, and T_0 and P_0 are a standard surface temperature and pressure. Figure 6d shows that for a given PotSR, surface area may change by a factor of 2 or more, and that increases in surface area are associated with lower values of m. Thus in PSCs the inference of surface area from SR measurements is somewhat uncertain. If surface area increases owing to water uptake, SR may not change much owing to decreases in particle index of refraction.

Volcanic Aerosol

Measurements in the Arctic by *Dye et al.* [1992] suggest that most sulfuric acid particles may still be liquid at temperatures below the equilibrium temperature for NAT and that condensation of NAT starts preferably on the larger aerosol particles, which have a higher probability to be frozen when the temperature drops under NAT saturation values. Dye et al. also observed that sulfuric acid aerosol can be supercooled to 190-192 K, close to the assumed homogeneous freezing temperature. This observation may help explain the high supersaturations over NAT often observed for the initiation of significant growth of PSC particles in the Arctic. While in the Arctic stratosphere very low temperatures are occasionally reached, in the Antarctic an examination of June through August analyses at 70 and 30 hPa show wide areas almost constantly below temperatures of 190 K. This finding suggests that at the end of winter all the Antarctic vortex air could have been cold enough to freeze the volcanic sulfuric acid droplets. Once frozen, the sulfuric acid aerosol is expected to remain frozen until temperatures warm to between 215 and 220 K [*Middlebrook et al.*, 1993], values uncommon in the late winter Antarctic stratosphere. Thus it is reasonable to assume that the volcanic aerosol droplets measured in late August and September were mostly frozen at the time of the measurements.

Figure 7 presents particle mixing ratio versus potential temperature for particles in the four categories as a function of particle size. In this figure, October 9 is presented separately from the volcanic category, because the characteristics of these particles differ somewhat from the volcanic aerosol measurements during the PSC period and because we are using October 9 to characterize the volcanic aerosol undisturbed by cold temperatures. Figure 7a gives the condensation nuclei (CN) mixing ratio, and Figures 7b through 7f show the mixing ratio within specific size intervals. Figure 7b was constructed from a comparison of the mixing ratio of particles of >0.15 μm with the CN measurement closest in time to the 0.15-μm measurement. As mentioned earlier and seen in Figure 7a, the three CN measurements were quite consistent. From the comparison of the concentration of particles between 0.01 and 0.15 μm on October 9 (Figure 7b) with the concentration of larger particles (Figures 7c to 7f) it appears that above 370 K (≈14-15 km) most of the small particles in the October 9 profile had earlier taken part in growth either through deliquescence of the volcanic aerosol or through nucleation and growth as NAW particles. The number of small (0.01-0.15 μm) particles is generally larger in the October 9 measurement than the other cases of volcanic and PSC aerosol. Below 1.0 μm the swelling of the cold volcanic aerosol is similar to the growth of NAWd. This similarity is lost for particles of >1.0 μm. The mixing ratio of all PSC particles between 1.0 and 2.0 μm increases by a factor of 10 to 100 above the volcanic aerosol. Above 2.0 μm the mixing ratio of NAWn returns to near-volcanic levels, while the mixing ratio of NAWd and ice remain elevated by factors of 10 to 100.

Gravitational sedimentation of the aerosol can be observed through changes in particle concentration as a function of potential temperature (altitude) for particles of >0.5 μm. The increasing mixing ratio for particles between 0.15 and 0.5 μm for all particle classes suggests very little vertical redistribution for particles of these sizes; however, above 350 K (≈12 km) the mixing ratio of the volcanic particles decreases quickly for sizes larger than 0.5 μm. During August and September inside the vortex, temperatures were always well below 200 K, and the volcanic aerosol cloud always contained a greater number of particles with radii >0.5 μm than was observed on October 9. In the October 9 observations, particle size distributions were bimodal below 15.5 km (415 K). The maximum SR, 2.7, was observed at approximately 11.5 km (340 K). At that altitude the total particle concentration was about 60 mg^{-1}, the second mode had a median radius of 0.44 μm, and the particles in the second mode were 23% of the total. At the bottom of the cloud, 10 km (320 K), the median radius of the second mode was shifted to around 0.7 μm, probably because of the increase in larger particles due to sedimentation, but the particles in the second mode were only 7.5% of the total number density. As was mentioned earlier, the errors in these sizes and concentrations associated with Poisson counting statistics are 10-20%.

Gravitational settling is not evident in the PSC particles, NAWn, NAWd, and ice. This finding is consistent with the relatively recent growth of these particles. For these types of particles the mixing ratios of 2.0 μm particles increase rapidly as altitude or potential temperature increases, reflecting the effect of decreasing temperature at these altitudes, which permits more water and nitric acid to be condensed on the particles. The volcanic aerosols are not expected to exhibit the same character as PSCs, since they may be expected to have a longer history as

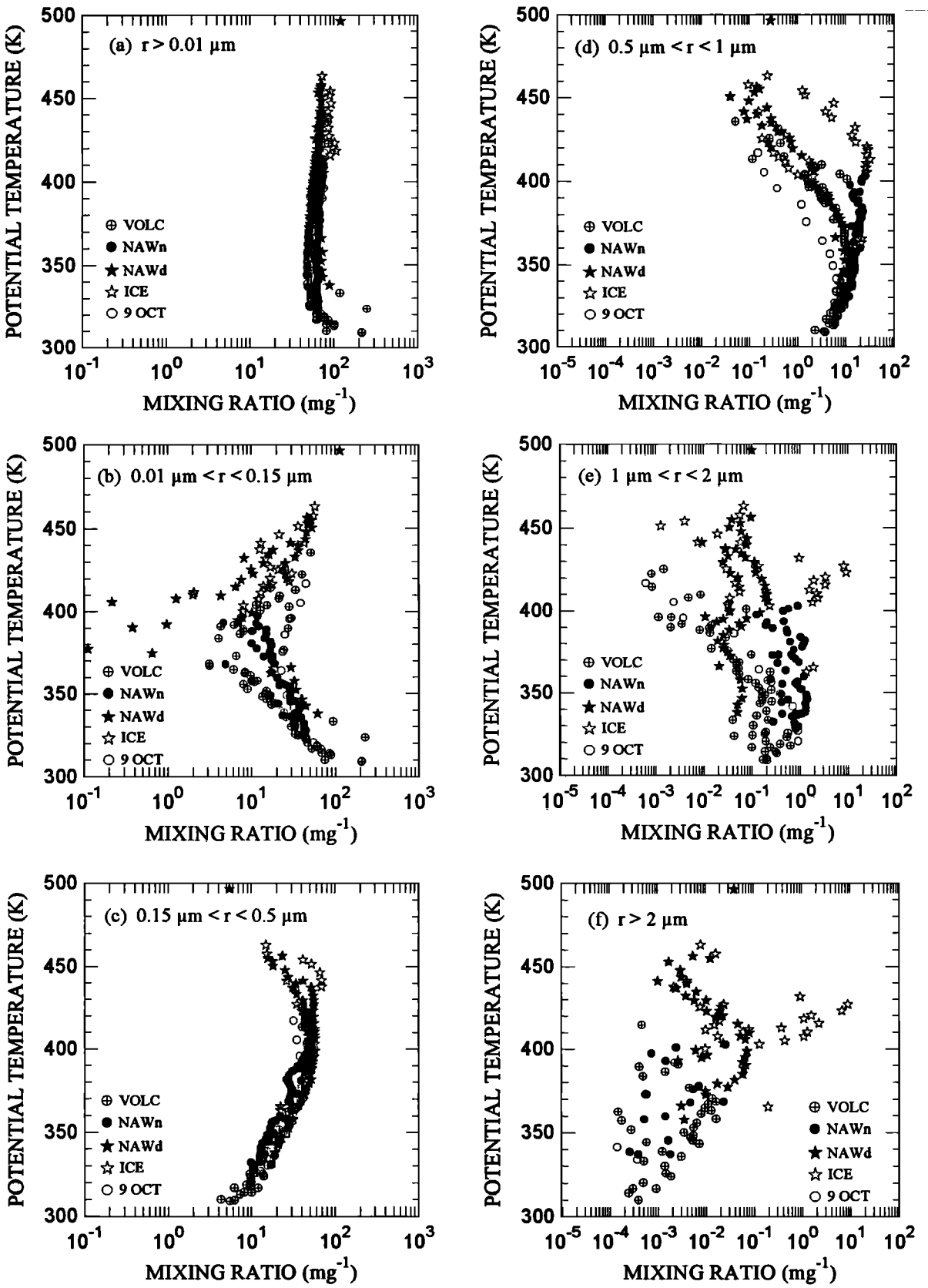

Figure 7. Vertical (potential temperature) profiles of mixing ratios in the size bins indicated. Only aerosols within the size bin indicated are included. The aerosol measurements are separated according to the classifications described in the text. October 9 is presented separately from the volcanic category.

stable larger particles due to deliquescence. Note that the volcanic aerosols with larger surface areas exhibit in general a lower index of refraction (Figures 5 and 6). Growth was observed on all particle sizes during the earlier volcanic measurements. During the October 9 measurements the average median radius of the first mode at various altitudes was about 0.2 μm, and the average median radius of the second mode, when present, about 0.6 μm. In the earlier volcanic measurements, average median radii were increased to about 0.3 and 1.6 μm, respectively.

The index of refraction for volcanic particles was found to be 1.43 ± 0.04 at 532 nm in the temperature range 190-203 K, which is in agreement with the calculations of *Steele and Hamill* [1981]. The refractive index was generally lower at low altitudes, where the concentration of water vapor would be higher, and water and possibly some nitric acid would be condensed on the surfaces. When temperature increases in late spring, the aerosol particles lose their water and nitric acid. The temperatures ranged around 202-205 K between 10 and 15 km where the volcanic aerosols were located. These temperatures were still low enough that sulfuric acid particles which had frozen during winter would not have melted. A residual depolarization of 2-2.4% was observed around the maximum SR between 11 and 13 km (Figure 2, 921009 panel).

Polar Stratospheric Clouds

On the third panel of Figure 1, equilibrium temperatures for NAT [*Hanson and Mauersberger*, 1988] and water ice are shown, assuming several vapor concentrations. During the observations, in situ concentrations of nitric acid were not available; however, water vapor was measured in late August in collaboration with S. Oltmans of the National Oceanic and Atmospheric Administration [*Deshler et al.*, 1994]. The water vapor mixing ratio was observed to decrease almost linearly, from 3.7 ppmv at 11 km to 1.5 ppmv at 19 km. This profile was assumed as a reference value between 12 and 20 km from late August until mid-September. Measurements performed in previous years during the same period gave values of 2-3 ppmv in this altitude range [*Hofmann et al.*, 1991]. An alternate method to infer water vapor content in the lower stratosphere is to use lidar observations of ice clouds formed by upward propagation of gravity waves or another significant cooling process. The temperatures in these clouds then correspond to the frost point temperature. In certain meteorological conditions the Transantarctic Mountains, often upwind of McMurdo, generate gravity waves. The ice clouds formed in these conditions are usually well defined in quite thin layers, often less than 1 km thick, and are characterized by high SR and high depolarization. The appearance of multilayer ice clouds (see Figure 2) on August 26 between 12 and 17 km at temperatures of 194 to 186 K, and on September 9 around 18 km at 186 K, suggest a water concentration around 3 ppmv, a little higher than, but close to, the measured water vapor profile in August.

An indication of the particle sizes affected by PSC growth can be obtained from Figure 7. Above 370 K (14-15 km), mixing ratios between 0.01 and 0.15 μm in all particle categories are lower than the October 9 volcanic aerosol. In contrast, at larger aerosol size ranges the PSC and volcanic aerosol categories contain mixing ratios higher than those on October 9. It appears that most of the particles found in the 0.01- and 0.15-μm size range during October 9 (assumed to be similar to the prewinter volcanic aerosol conditions) grew to larger sizes over the winter inside the vortex.

In Figure 8 the temperatures observed during the lidar particle counter comparisons are reported as a function of altitude and SR. PSCs were observed at temperatures lower than 196 K even at the lowest altitudes (12 km), except for measurements performed on September 14 (920914 in Figure 2) represented by the five black stars in Figure 8 that appear at temperatures higher than 196 K. This measurement will be discussed in more detail later. Comparing temperatures measured over McMurdo during PSC events with equilibrium existence temperatures for NAT

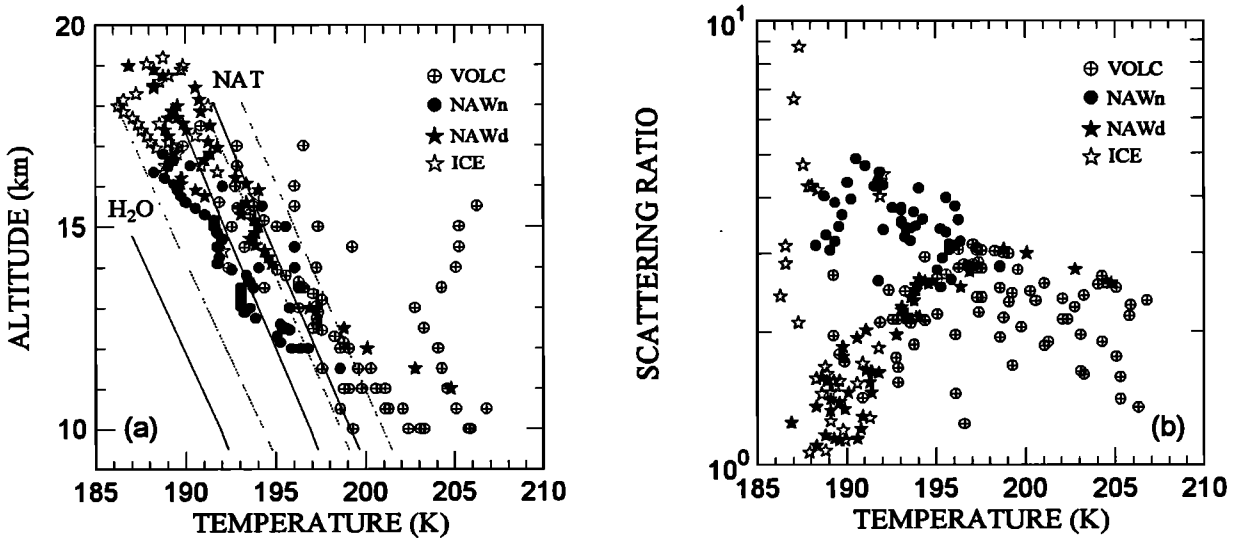

Figure 8. Temperature versus (a) altitude and (b) SR measured during the lidar and particle counter comparisons, grouped into the four categories. In Figure 8a, equilibrium existence temperatures for NAT and water for 1 and 5 ppbv HNO_3, with 2 (solid lines) and 3 (dashed lines) ppmv H_2O are included.

from *Hanson and Mauersberger* [1988], assuming a water vapor concentration of 3 ppmv below 18 km, the concentration of nitric acid in the lower stratosphere can be roughly estimated at 1-2 ppbv. These values are in good agreement with HNO_3 measurements from the CLAES instrument on the upper atmospheric research satellite [*Roche et al.*, 1993]. From Figure 8 it is also clear that NAWn were usually observed in the coldest temperature range at a particular altitude and are thus perhaps associated with faster cooling rates. Measurements performed during 1991 [*Adriani et al.*, 1992] show that for moderate cooling rates, lower than 5-6 K day^{-1}, PSCs have a higher depolarization and a relatively lower SR. In such conditions the formation of NAWd seems to be promoted.

To evaluate the temperature history of air parcels containing PSCs observed at McMurdo, back trajectories were calculated by using a three-dimensional transport trajectory model [*Kallberg*, 1988] and data over Antarctica from the European Center for Medium-Range Weather Forecasts (ECMWF, Reading, England). Because of questions concerning the accuracy of the vertical component of the wind in three-dimensional trajectory models, isentropic models are more commonly used for back trajectories. Comparisons between isentropic and three-dimentional models in describing air parcel history indicate no major differences in the longitude-latitude plane, but possible errors in the temperature history of the air parcel [*Austin and Tuck*, 1985; *Martin et al.*, 1987]. For several cases we have compared temperature history from Kallberg's model with an isentropic trajectory model and found no major differences. The choice of the three-dimensional model was based on its availability. For detailed analysis, 24 trajectories were chosen to cover the four particle classes. Four trajectories each from six of the seven comparative measurement days were chosen. They are represented by the solid circles in Figure 2 and include 8 trajectories for NAWn, 10 for NAWd, 3 for ice, and 3 for volcanic aerosol. The trajectories are reported in Figures 9 and 10 for the August and September measurements. For the same back trajectories, Figure 11 reports SR, depolarization, particle surface area, and index of refraction as a function of various parameters related to the thermal history of the air parcel. The cooling rates in Figure 11 are based on temperature changes over a 6-hour period. Figure 12 reports thermal histories during the last 5 days for the data shown in Figure 11.

Figures 9 and 10 show two main kinds of trajectories, some with significant excursions to lower latitudes, approaching 60°S, and others confined to higher latitudes, south of 70°S. As air parcels move to lower latitudes, their altitude decreases, with a corresponding increase of temperature. In contrast, air parcels moving to higher latitudes can be rapidly cooled by ascent, inducing cloud formation. The trajectories in the 48 hours prior to observations on August 29 (138 and 108 mb) and September 9 (both observations) were quite similar. In all cases the air parcels moved from latitudes near 65°S to McMurdo at 78°S, and clouds classified as NAWn and ice were observed. Figure 11a shows large cooling rates, between 7 and 20 K day^{-1}, for these observations. The displacement of the air parcel to higher latitudes and the consequent altitude increase as the air parcel passes deeper into the vortex at least partially account for the rapid temperature drop.

The potential temperature (altitude) dependence of SR, depolarization, and surface area is shown in Figure 13. From Figures 5c and 13c the surface area densities in NAWn and ice clouds are the highest among the PSCs measured during spring 1992. This fact could suggest that during the passage at low latitude an exchange of air with the outer vortex stratosphere permitted enrichment of the air mass in terms of nitric acid and water vapor and thus increased the vapors available for condensation. Figure 11, associating NAWn with fast cooling, and Figure 7, associating NAWn with the growth of a higher percentage of particles of <0.5 μm to sizes of >0.5 μm, together suggest that during fast cooling a higher fraction of the volcanic aerosol takes part in the condensation of NAW, and on the basis of the low depolarization observed these particles are more likely to be amorphous or ternary solution droplets. In the 0.5- to 2.0-μm range the highest number concentrations are observed in PSCs classified as NAWn (Figures 7d and 7e). The growth of particles of >2 μm, in cases of fast cooling, appears to be mainly related to ice cloud formation, producing large aspherical particles. The average temperature during the previous 5 days for air parcels producing NAWn and ice was always warmer than that at the time of the observation at McMurdo (Figures 11d and 12), and there was a strong latitudinal dependence (Figure 11e).

The history of air parcels producing NAWd was quite different. The warm temperatures observed in trajectories leading to NAWn were not observed in trajectories leading to NAWd, and the trajectories remained closer to the Antarctic continent. For NAWd the temperature was usually low enough, <195 K, to sustain or grow particles of >2 μm, while cooling rates were lower, typically <5 K day^{-1} and never greater than 8-9 K day^{-1}. When, in some cases, the temperature increased during the last part of the trajectory, it was not sufficient to evaporate the larger particles (Figure 7f).

Some NAWd features are similar to volcanic aerosol, and it can be difficult to distinguish between them. The biggest differences are in depolarization and in the concentration of the larger particles. In Figure 7 the substantial difference between NAWd and volcanic aerosol is in the concentration of particles of >1 μm. For NAWd the concentration of particles of >2 μm is greater than all other cases except for the ice clouds. In Figures 13a, and 13c the volcanic aerosol and NAWd have similar SR and surface area characteristics; however, the NAWd has a clearly different depolarization signal (Figure 13b). General characteristics of the PSC observations in terms of concentration, surface area, and volume of particles larger than 2 μm are given in Table 2, along with 48-hour cooling rate.

The points in Figure 8 classified as NAWd at temperatures higher than 196 K were so classified because of the high values of depolarization and low SR. Those points correspond to observations on September 14 (Figure 2) when the temperature was too warm to sustain PSCs (Figure 8a) at altitudes below 370 K, 13.5 km. The measurements on this day indicated the highest concentrations of particles between 0.01 and 0.15 μm (Figure 7b), the lowest concentrations of particles of >0.5 μm (Figures 7d and 7e), and no particles of >2.0 μm (Figure 7f). Yet this case also produced a SR higher than all the other volcanic measurements (Figures 8b and 13a). Evidently, there were many small aspherical particles producing a relatively high SR (2.5-3) and

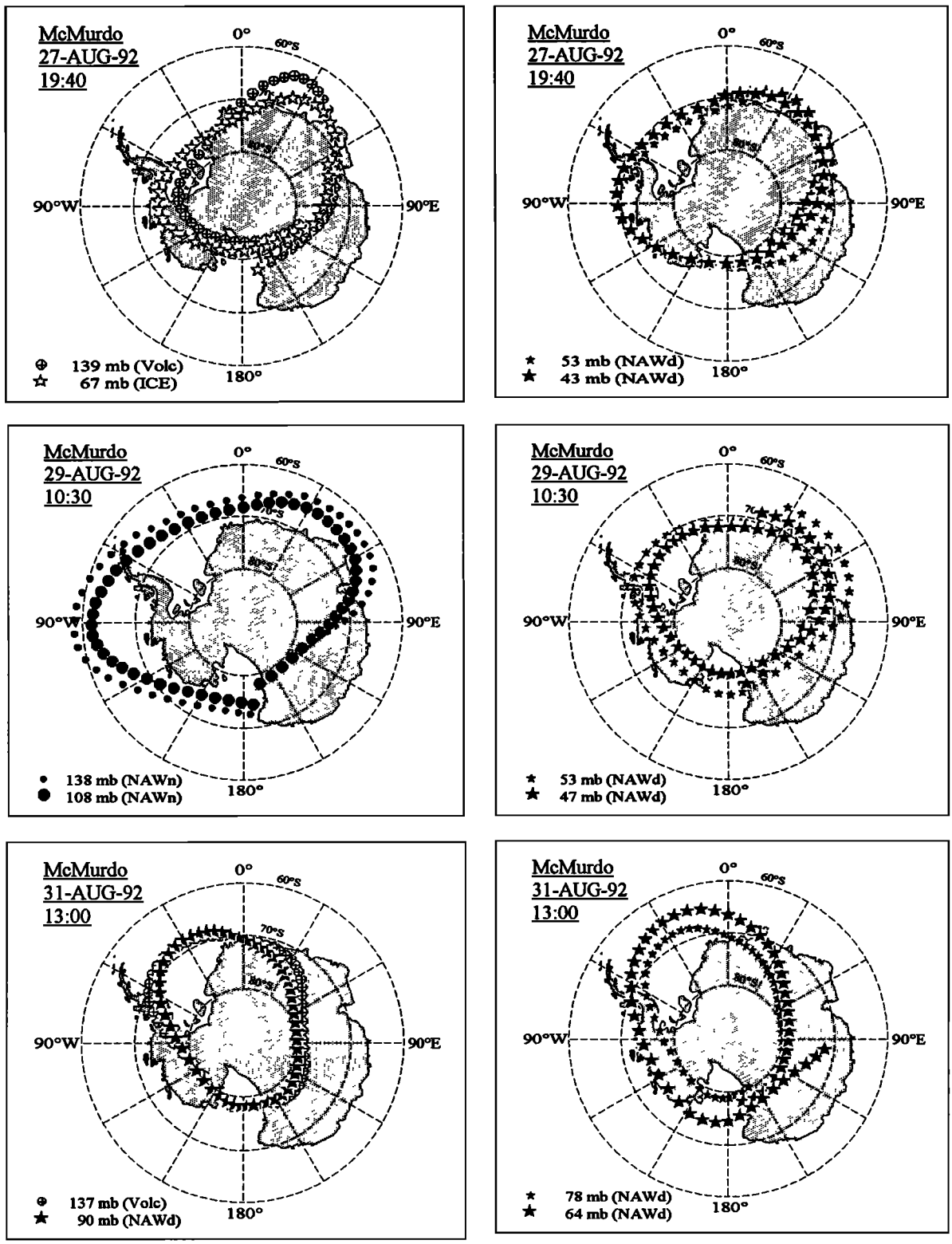

Figure 9. Air parcel back-trajectories calculated for August 27, 29, and 31, 1992, using a three-dimensional transport model. All the trajectories extend back 7 days from the labeled dates.

high depolarization (3-6%). This phenomena was observed for a few days around mid-September.

The unusual particles observed on September 14 coincided with unusual trajectories as well. The vortex shape was elliptical, and air over McMurdo had come from latitudes of 60°S within a few days (Figure 10). Details of the trajectory coinciding with the peak in depolarization, 12.5 km, observed on September 14 are shown in Figure 14. About 6 days before observation the air mass approached the pole with cooling rates of 4-5 K day^{-1} and the temperature decreased to about 188 K.

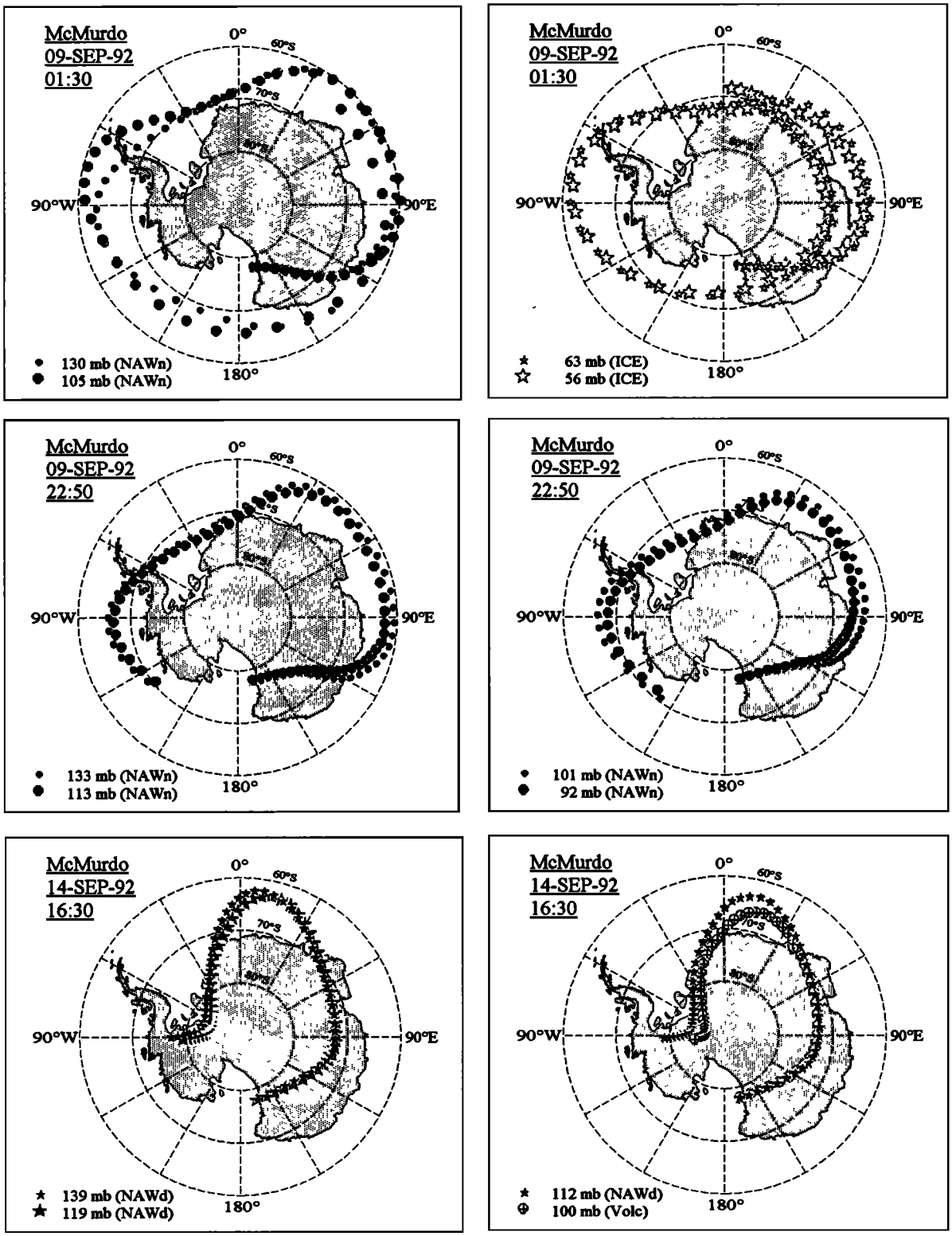

Figure 10. Air parcel back trajectories calculated for September 9 and 14, 1992. All the trajectories extend back 7 days from the labeled dates.

The parcel was then warmed by a displacement to lower latitudes and temperatures higher than 200 K (heating rates of 8 K day^{-1}) before experiencing a new cooling at the rate of about 6 K day^{-1} to 195 K. The temperature remained constant around 195 K for about 60 hours, which, at that altitude, is low enough for NAT formation, assuming 1 ppbv HNO_3 and 2-3 ppmv H_2O, before rapidly increasing to 200 K in the last 12 hours. The temperature at the time of the observation, 200 K, was equivalent to the NAT existence temperature, assuming 3 ppmv H_2O and 5 ppbv HNO_3; however, below 12 km the temperature was 3-5 K above the equilibrium existence temperature for NAT particles at those altitudes (Figure 8a). This fact suggests that the particles formed

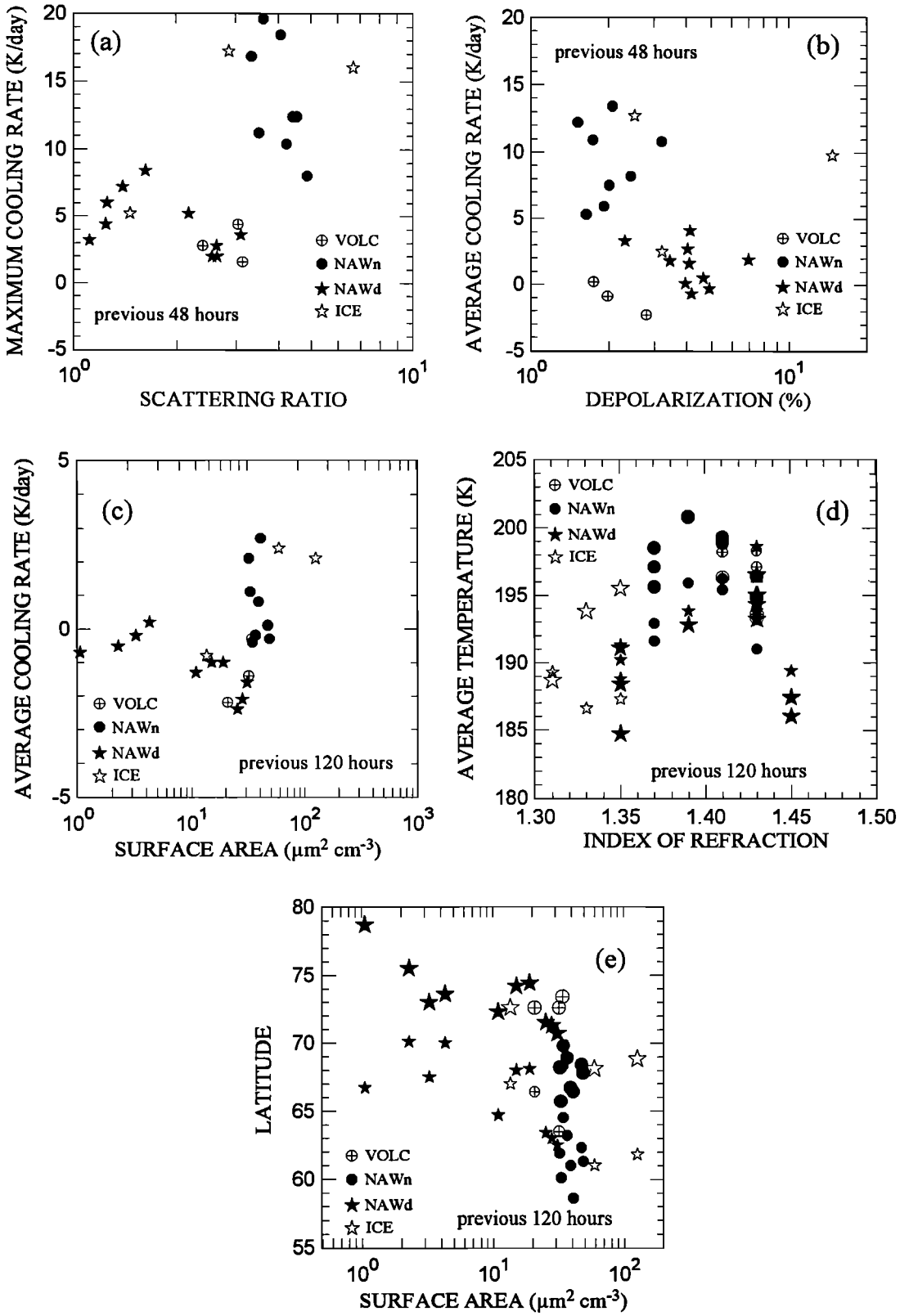

Figure 11. a) Maximum cooling rate experienced in the 48 hours preceding the observations. (b) Average cooling rates during the 48 hours preceding the observations. (c) Average cooling rates during the 5 days preceding the observations. (d) Average temperatures during the 5 days preceding the observations (large symbols) and temperatures at the time of the observations (small symbols). (e) Minimum latitude crossed by the air parcel in the previous 5 days (small symbols) and average latitude in last 5 days (large symbols).

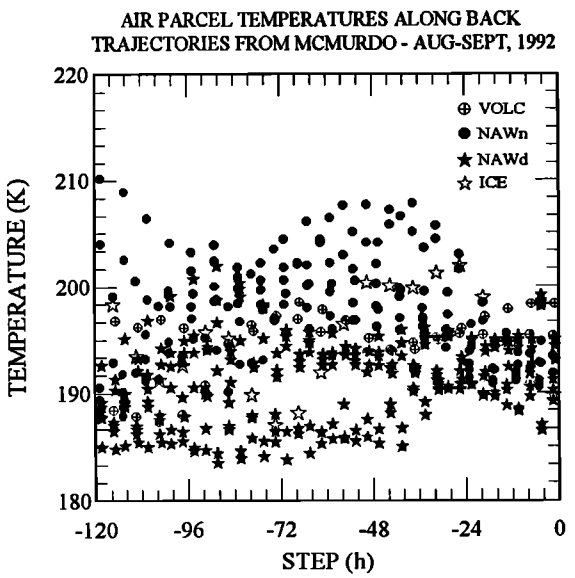

Figure 12. Air parcel temperatures experienced during the 5 days prior to the observations over McMurdo.

during the previous 60 hours at 195 K and that a significant fraction of the nonspherical or crystalline particles had not completely evaporated during the 12-hour period in which the temperatures warmed to 200 K, or that the H_2O and HNO_3 vapor concentrations are significantly higher below 12 km. If the first of these two possibilities is the case, then this evidence supports the idea that PSC particles may undergo a slow evaporation process due to a nitric acid coating [*Peter et al.*, 1994]. At the level of maximum depolarization, 350 K (≈12.5 km), no particles of >2.0 μm were observed (Figure 7f). Just a few particles of >2.0 μm (≈$3x10^{-3}$ mg^{-1}) were observed around 360 K (13-13.5 km).

Some trajectories during the last days of August (profiles from August 27 to 30 in Figure 2) have been partially discussed by *Gobbi and Adriani* [1993]. Between 16 and 21 km, potential temperatures of 400-500 K, PSCs with high depolarizations and low SRs were observed. Those clouds were mostly classified as NAWd. The temperature history at these times indicated that the temperature remained between 185 and 190 K during the week preceding the observations with a slight warming, but not above 195 K, during the last 48 hours (Figure 12). The situation suggests that sustained low temperatures over the previous 5 days promoted the growth of a few large particles (Figure 7).

Figure 15 gives a survey of all the lidar measurements depicted in Figure 2 except for those reported in the lidar particle counter comparisons. The individual measurements are classified on the basis of the same criteria used before and described in Figure 1. The temperature at which ice particles were observed (Figure 2, 920826, 920908, 920909, and Figure 15c) indicates a value of 3-4 ppmv for the water vapor concentration between 13 and 18 km for the measurement period. The coldest temperatures were recorded at the end of August and in the period September 8-10. The analysis of the temperatures with respect to altitude and SR show that PSCs were observed at temperatures lower than 198 K and at altitudes above 11 km. In all the PSC observations, temperatures were below the NAT condensation temperatures for 3 ppmv water vapor and 5 ppbv nitric acid.

Summary and Conclusions

Observations of stratospheric clouds were performed in Antarctica by lidar in the period August 26 to October 9, 1992. In the same period, seven measurements were coordinated with particle counters released on balloons. The two types of measurements were compared by using the size distribution measurements from the particle counter to calculate a lidar scattering ratio and then adjusting the particle index of refraction until the calculated and measured SR were in agreement. The aerosol measurements were classified into volcanic aerosol and PSCs. The volcanic aerosol contained all measurements with lidar profiles similar to the final profile of the season, October 9.

Very cold temperatures occur throughout the Antarctic stratosphere during the months of July and August. As a result, volcanic aerosols within the polar vortex are expected to be mostly frozen and to remain frozen for the Antarctic spring, furnishing the sites for growth of PSC particles. A low residual depolarization, 2-2.4%, for the volcanic aerosol measurements supports this idea. This low residual depolarization persisted through the final measurements in October, even though the size distribution of the volcanic particles had changed significantly through the period, containing fewer large, and a relatively greater number of small (<0.5 μm) particles. In late August and in September inside the polar vortex, the volcanic clouds contained particles greater than 1.0 μm in radius. The refractive index inferred for these measurements was 1.43 ± 0.04, consistent with the index expected on the basis of the temperatures and water vapor concentrations within the vortex.

PSCs were observed to appear within the volcanic aerosol layer at temperatures below 198 K and above 11 km. The temperature at which ice and non-ice clouds were observed in the period August 26 to September 9 indicated a concentration of 3 ppmv water vapor and 1-2 ppbv nitric acid in the range 12-18 km. The PSCs were further subdivided into three categories

Table 2. Mixing Ratios, Surface Areas, and Volumes of Particles Larger Than 2 μm Radii in Polar Stratospheric Clouds

	Mixing Ratio, mg^{-1}	Surface Area, $\mu m^2 cm^{-3}$	Volume, $\mu m^3 cm^{-3}$	Cooling Rate Range, K day^{-1}
NAWn	<0.006	0.00008-0.3	0.00006-0.2	8-20
NAWd	0.001-0.06	0.0004-0.7	0.0003-0.5	1-8
ICE	0.01-9.0	1.9-62	1.7-40	5-18

The cooling rates are averaged on the previous 48 hours.

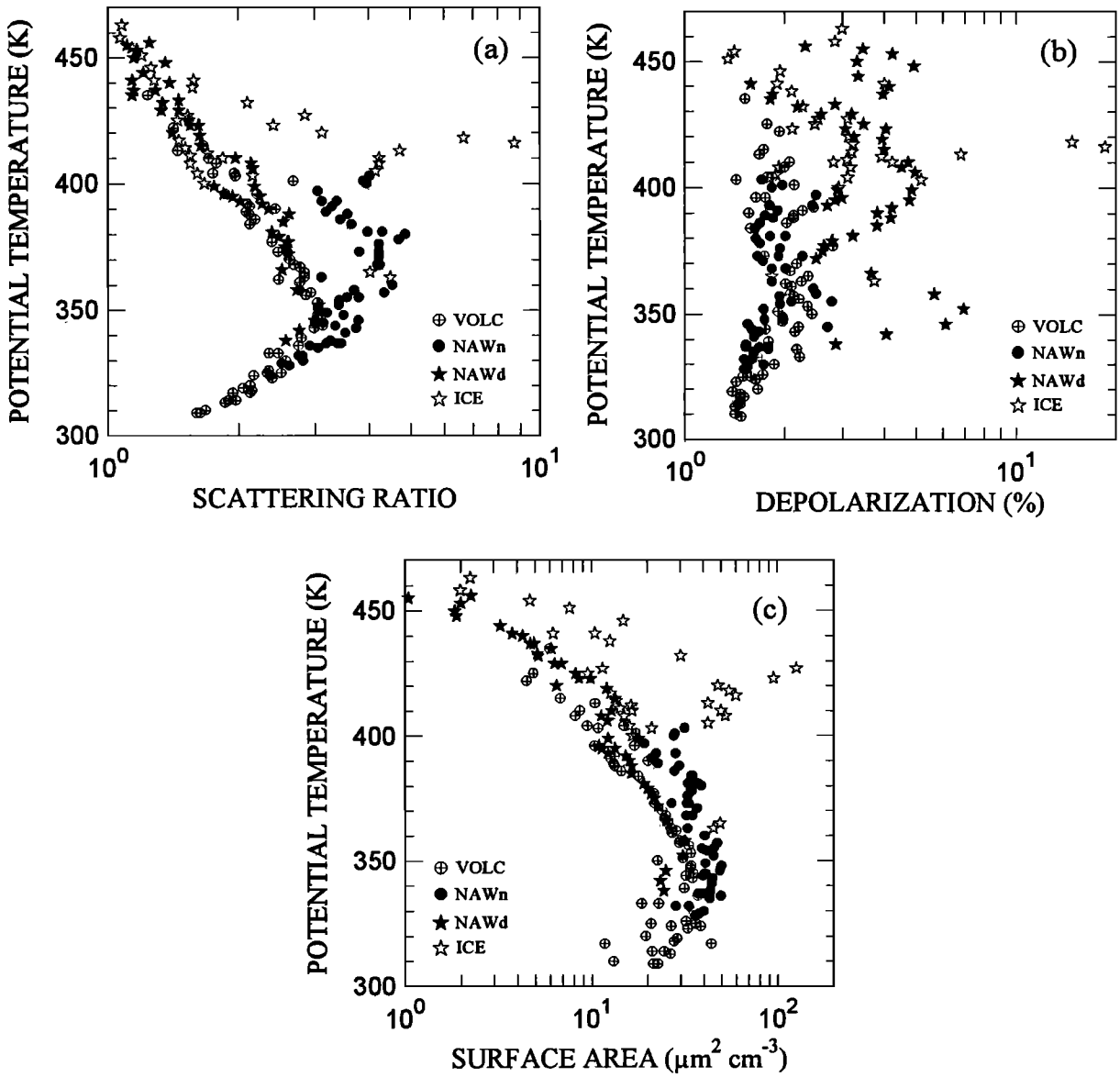

Figure 13. Vertical (potential temperature) profiles of (a) SR, (b) depolarization, and (c) surface area density (μm^2 cm^{-3}) during the lidar particle counter comparisons. The measurements are separated into the four categories.

based on their lidar signature: non-ice PSCs with moderate SR and low depolarization, non-ice PSCs with a low SR but high depolarization, and ice with high SR and high depolarization. The distributions of index of refraction at a wavelength of 532 nm for the non-ice PSCs led to means of 1.39 ± 0.03 for the nondepolarizing class and 1.42 ± 0.04 for the depolarizing class. The modes were 1.37 and 1.43, respectively. Comparison with laboratory measurements of index of refraction of HNO_3/H_2O films suggests that the indices of refraction for these classes are consistent with laboratory results for an amorphous particle with stoichiometry similar to a tri- or higher hydrate, or with the lower range of measurements on crystalline nitric acid trihydrate. The distribution of index of refraction for ice led to a mean of 1.32 ± 0.01 and a mode of 1.31, in close agreement with accepted values.

Fast cooling (>7 K day^{-1}) seems to produce the nondepolarizing clouds, when most of the underlying stratospheric particles participate in the growth of PSC particles, but very few particles grow as large as 2.0 μm. Except for the ice clouds the nondepolarizing clouds produced the highest SR (2.5-5) and surface area density (50 μm^2 cm^{-3}), peaking at altitudes between 340 and 370 K (12 and 16 km). Only when temperatures were below the NAT equilibrium temperature for a long time, or reached the ice point, were significant concentrations of particles of >2.0 μm observed. On the basis of the higher depolarizations observed in these cases, some of the particles are expected to have aspherical shapes. In these cases, cooling below the frost point leads to the formation of ice, while slow cooling to sustained temperatures just above the frost point leads to the development of a depolarizing cloud with low SR. In one case, rapid heating of these

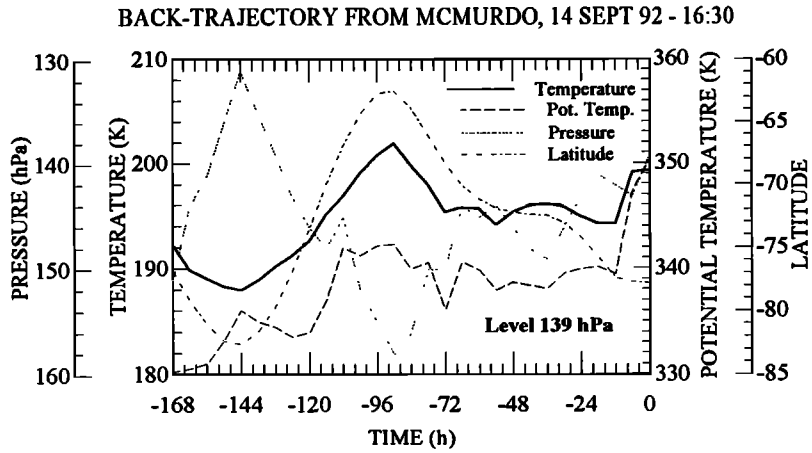

Figure 14. Back-trajectory temperature, potential temperature, pressure, and latitude of the air parcel at 12.5 km which arrived at McMurdo on September 14.

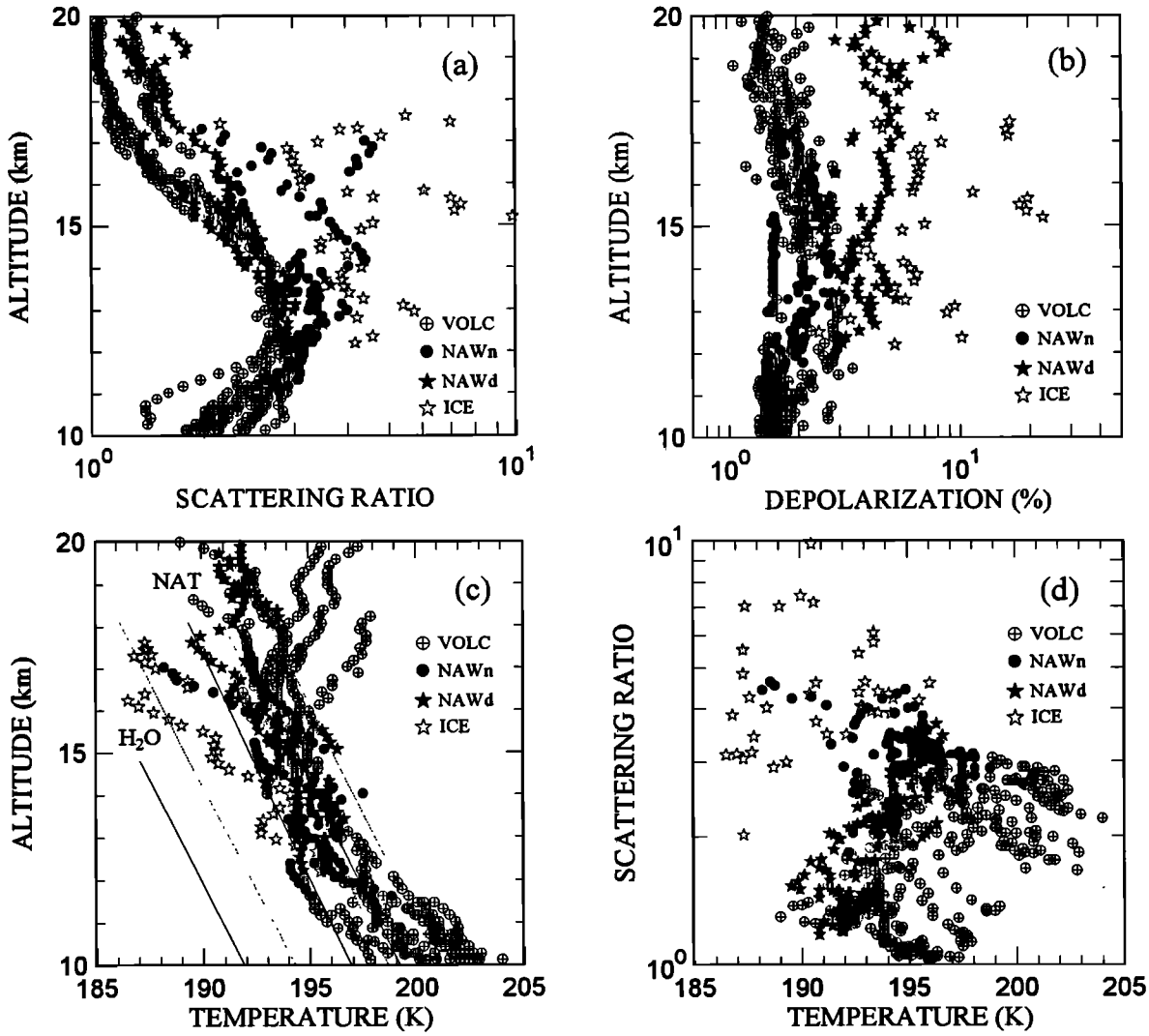

Figure 15. Vertical (altitude) profiles of (a) SR, (b) depolarization, (c) temperature for the lidar measurements not performed along with the particle counter flights, and (d) temperature as a function of SR for these same flights. By using the categories as for the lidar particle counter comparisons, these measurements are separated into the same four classes. The equilibrium existence temperatures are for 1 and 5 ppbv HNO_3, with 2 (dashed lines) and 3 (solid lines) ppmv H_2O.

clouds, over periods of 12-24 hours, did not cause evaporation of all the particles.

Even though for the nondepolarizing high SR clouds and the cold volcanic aerosol there was a general pattern of a linear increase of surface area with SR, closer inspection revealed that at a specific SR, as surface area increased, index of refraction decreased. This finding is consistent with water being the primary species condensed during particle growth and would be expected for both the deliquescence of volcanic aerosol at cold temperatures and the condensation of nitric acid in PSCs. Further evidence of this pattern was observed as an approximate doubling of surface area density as estimated index of refraction decreased from 1.45 to 1.3.

Broadly speaking, these measurements indicate four classes of winter polar stratospheric aerosol. Below a potential temperature of 400 K (16-17 km), volcanic aerosol and nondepolarizing hydrated nitric acid particles were predominant with surface areas in the range of 10-30 and 20-50 μm^2 cm^{-3}, respectively. Above 400 K, depolarizing hydrated nitric acid and ice clouds were predominant with surface areas of 5-15 and 5-100 μm^2 cm^{-3}. Future work will extend this analysis to joint measurements over McMurdo Station collected in 1993 and 1994.

Acknowledgments. This research was supported by the Italian National Program for Antarctic Research and the U. S. National Science Foundation. Gratitude is extended to L. Womack, B. Johnson, and W. Rozier for completing the particle counter measurements in Antarctica. We are also grateful for discussions with Stephan Borrmann and for thorough reviews which contributed significantly to the manuscript.

References

Adriani, A., T. Deshler, G. P. Gobbi, B. J. Johnson, and G. Di Donfrancesco, Polar stratospheric clouds over McMurdo, Antarctica, during the 1991 spring: Lidar and particle counter measurements, *Geophys. Res. Lett., 19*, 1755-1758, 1992.

Anthony, S. E., R. T. Tisdale, R. S. Disselkamp, M. A. Tolbert, and J. C. Wilson, FTIR studies of low temperature sulfuric acid aerosols, *Geophys. Res. Lett., 22*, 1105-1108, 1995.

Arnold, F., Stratospheric aerosol increases and ozone destruction: Implications from mass spectrometer measurements, *Ber. Bunsenges. Phys.Chem., 96*, 339-350, 1992.

Austin, J., and A. F. Tuck, The calculation of stratospheric air parcel trajectories using satellite data, *Q. J. R. Meteorol. Soc., 111*, 279-307, 1985.

Berland, B. S., D. R. Haynes, K. L. Foster, M. A. Tolbert, S. M. George, and O. B. Toon, Optical Characterization of model stratospheric clouds: Refractive indices of amorphous and crystalline HNO_3/H_2O films, *J. Phys. Chem., 98*, 4358-4364, 1994.

Beyer, K. D., S. W. Seago, H. Y. Chang, and M. J. Molina, Composition and freezing of aqeous H_2SO_4/HNO_3 solutions under polar stratospheric conditions, *Geophys. Res. Lett., 21*, 871-874, 1994.

Browell, E. V., C. F. Butler, S. Ismail, P. A. Robinette, A. F. Carter, N. S. Higton, O. B. Toon, M. R. Schoeberl, and A. F. Tuck, Airborne lidar observations in the wintertime Arctic stratosphere: Polar stratospheric clouds, *Geophys. Res. Lett., 17*, 385-388, 1990.

Carslaw, K. S., B. P. Luo, S. L. Clegg, T. Peter, P. Brimblecombe, and P. J. Crutzen, Stratospheric aerosol growth and HNO_3 and water uptake by liquid particles, *Geophys. Res. Lett., 21*, 2479-2482, 1994.

Crutzen, P. J., and F. Arnold, Nitric acid cloud formation in the cold Antarctic stratosphere: A major cause for the springtime ozone hole, *Nature, 324*, 651-654, 1986.

Deshler, T., In situ measurements of Pinatubo aerosol over Kiruna on four days between January 18 and February 13, 1992, *Geophys. Res. Lett., 21*, 1323-1326, 1994.

Deshler, T., A. Adriani, D. J. Hofmann, and G. P. Gobbi, Evidence for denitrification in the 1990 Antarctic spring stratosphere; 2, Lidar and aerosol measurements, *Geophys. Res. Lett., 18*, 1999-2002, 1991.

Deshler, T., A. Adriani, G.P. Gobbi, D. J. Hofmann, G. Di Donfrancesco, and B. J. Johnson, Volcanic aerosol and ozone depletion within the Antarctic polar vortex during the austral spring of 1991, *Geophys. Res. Lett., 19*, 1819-1822, 1992.

Deshler, T., B. J. Johnson, and W. R. Rozier, Balloonborne measurements of Pinatubo aerosol during 1991 and 1992 at 41°N: Vertical profiles, size distribution, and volatility, *Geophys. Res. Lett., 20*, 1435-1438, 1993.

Deshler, T., B. J. Johnson, and W. R. Rozier, Changes in the character of polar stratospheric clouds over Antarctica in 1992 due to the Pinatubo volcanic aerosol, *Geophys. Res. Lett., 21*, 273-276, 1994.

Drdla, A., A. Tabazadeh, R. P. Turco, M. Z. Jacobsen, J. E. Dye, C. Twohy, and D. Baumgardner, Analysis of the physical state of one Arctic polar stratospheric cloud based on observations, *Geophys. Res. Lett., 21*, 2475-2478, 1994.

Dye, J. E., D. Baumgardner, B. W. Gandrud, S. R. Kawa, K. K. Kelly, M. Loewenstein, G. V. Ferry, K. R. Chan, and B. L. Gary, Particle size distribution in Arctic polar stratospheric clouds, growth and freezing of sulfuric acid droplets, and implications for cloud formation, *J. Geophys. Res., 97D*, 8015-8034, 1992.

Fahey, D. W., K. K. Kelly, G. V. Ferry, L. R. Poole, J. C. Wilson, D. M. Murphy, M. Loewenstein, and K. R. Chan, In situ measurements of total reactive nitrogen, total water, and aerosol in a polar stratospheric cloud in the Antarctic, *J. Geophys. Res., 94*, 11,299-11,316, 1989.

Farman, J. C., B. G. Gardiner, and J. D. Shanklin, Large losses of total ozone in Antarctica reveal seasonal ClO_x/NO_x interaction, *Nature, 315*, 207-201. 1985.

Gable, C. M., H. F. Betz, and S. H. Maron, Phase equilibria of the system sulfur trioxide-water, *J. Am. Chem. Soc., 72*, 1445-1448, 1950.

Gobbi, G. P., and A. Adriani, Mechanisms of formation of stratospheric clouds observed during the Antarctic late winter of 1992, *Geophys. Res. Lett., 20*, 1427-1430, 1993.

Godin, S., G. Megie, C. David, D. Haner, C. Flesia, and Y. Emery, Airborne lidar observations of mountain-wave-induced polar stratospheric clouds during EASOE, *Geophys. Res. Lett., 21*, 1335-1338, 1994.

Hanson, D. R., and K. Mauersberger, Laboratory studies of the nitric acid trihydrate: Implication for the south polar stratosphere, *Geophys. Res. Lett., 15*, 855-858, 1988.

Hofmann, D. J., and T. Deshler, Comparison of stratospheric clouds in the Antarctic and the Arctic, *Geophys. Res. Lett., 16*, 1429-1432, 1989.

Hofmann, D. J., and T. Deshler, Stratospheric cloud observations during formation of the Antarctic ozone hole in 1989, *J. Geophys. Res., 96*, 2897-2912, 1991.

Hofmann, D. J., J. M. Rosen, J. W. Harder, and J. V. Hereford, Balloon-borne measurements of aerosol, condensation nuclei, and cloud particles in the stratosphere at McMurdo Station, Antarctica, during the spring of 1987, *J. Geophys. Res., 94*, 11,253-11,270, 1989.

Hofmann, D. J., T. Deshler, F. Arnold, and H. Schlager, Balloon observations of nitric acid aerosol formation in the Arctic stratosphere; 2, Aerosol, *Geophys. Res. Lett., 17*, 1279-1282, 1990.

Hofmann, D. J., S. J. Oltmans, and T. Deshler, Simultaneous balloon-borne measurements of stratospheric water vapor and ozone in the polar regions, *Geophys. Res. Lett., 18*, 1011-1014, 1991.

Iraci, L. T., A. M. Middlebrook, M. A. Wilson, and M. A. Tolbert, Growth of nitric acid hydrates on thin sulfuric acid films. *Geophys. Res. Lett., 21*, 867-870, 1994.

Jensen, E. J., O. B. Toon, and P. Hamill, Homogeneous freezing nucleation of stratospheric solution droplets, *Geophys. Res. Lett., 18*, 1857-1860, 1991.

Johnson, B. J., T. Deshler, and W. R. Rozier, Ozone profiles at McMurdo Station, Antarctica, during the austral spring of 1992, *Geophys. Res. Lett., 21*, 269-272, 1994.

Kallberg P., Kinematic air parcel trajectory, report, Eur. Cent. for Medium-Range Weather Forecasts, Reading, England, 1988.

Kawa, S. R., D. W. Fahey, K. K. Kelly, J. E. Dye, D. Baumgardner, B. W. Gandrud, M. Loewenstein, G. V. Ferry, and K. R. Chan, The Arctic polar stratospheric cloud aerosol: Aircraft measurements of reactive nitrogen, total water, and particles, *J. Geophys. Res., 97*, 7925-7938, 1992.

Kent, G. S., L. R. Poole, M. P. McCormick, S. K. Schaffner, W. H. Hunt, and M. T. Osborn, Optical backscatter characteristics of Arctic polar stratospheric cloud, *Geophys. Res. Lett., 17,* 377-380, 1990.

Koehler, B. G., A. M. Middlebrook, and M. A. Tolbert, Characterization of model polar stratospheric cloud films using Fourier transform infrared spectroscopy and temperature programmed desprption, *J. Geophys. Res., 97,* 8065-8074, 1992.

Larsen, N., J. M. Rosen, N. T. Kjome, and B. Knudsen, Deliquescence and freezing of stratospheric aerosol observed by balloon-borne backscattersondes, *Geophys. Res. Lett, 22,* 1233-1236, 1995.

Luo, B. P., T. Peter, and P. J. Crutzen, Freezing of stratospheric aerosol droplets, *Geophys. Res. Lett., 21,* 1447-1450, 1994.

Marti, J., and K. Mauersberger, Laboratory simulations of PSC particle formation, *Geophys. Res. Lett., 20,* 359-362, 1993.

Martin, D., C. Mithieux, and B. Strauss, On the use of the synoptic vertical wind component in the transport trajectory model, *Atmos. Environ., 21,* 45-52, 1987.

McCormick, M. P., H. M. Steele, P. Hamill, W. P. Chu, and T. J. Swissler, Polar stratospheric cloud sightings by SAM II, *J. Atmos. Sci., 39,* 1387-1397, 1982.

Middlebrook, A. M., L. T. Iraci, L. S. McNeill, B. G.Koehler, O. W. Saastad, M. A. Tolbert, and D. R. Hanson, FTIR studies of thin H_2SO_4/H_2O films: Formation, water uptake, and solid-liquid phase changes, *J. Geophys. Res., 98,* 20,473-20,481, 1993.

Middlebrook, A. M., B. S. Berland, S. M. George, M. A. Tolbert, and O. B. Toon, Real refractive indices of infrared-characterized nitric acid/ice films: Implications for optical measurements of polar stratospheric clouds, *J. Geophys. Res., 99,* 25,655-25,666, 1994.

Molina, M. J., R. Zhang, P. J. Wooldridge, J. R. McMahon, J. E. Kim, H. J. Chang, and K. B. Beyer, Physical chemistry of the $H_2SO_4/HNO_3/H_2O$ system: Implications for polar stratospheric clouds, *Science, 261,* 1418-1423, 1993.

Peter, T., P. J. Crutzen, R. Müller, and T. Deshler, The lifetime of leewave-induced ice particles in the Arctic stratosphere; 2, Stabilization due to NAT coating, *Geophys. Res. Lett., 22,* 1331-1334, 1994.

Poole, L. R., and M. P. McCormick, Airborne lidar observations of Arctic polar stratospheric clouds: Indications of two distinct growth stages, *Geophys. Res. Lett., 15,* 21-23, 1988.

Poole, L. R., G. S. Kent, M. P. McCormick, W. H. Hunt, M. T. Osborn, S. Schaffner, and M. C. Pitts, Dual-polarization airborne lidar observations of polar stratospheric cloud evolution, *Geophys. Res. Lett., 17,* 389-392, 1990.

Pueschel, R. F., et al., Condensed nitrate, sulfate, and chloride in Antarctic stratospheric aerosols *J. Geophys. Res., 94,* 11,271-11,284, 1989.

Roche, A. E., J. B. Kumer, and J. L. Mergenthaler, CLAES observations of $ClONO_2$ and HNO_3 in the Antarctic stratosphere between June 15 and September 17, 1992, *Geophys. Res. Lett., 20,* 1223-1226, 1993.

Rosen, J. M., S. J. Oltmans, and W. F. Evans, Balloon-borne observations of PSCs, frost point, ozone, and nitric acid in the north polar vortex, *Geophys. Res. Lett., 16,* 791-794, 1989.

Rosen, J. M., N. T. Kjome, and S. J. Oltmans, Simultaneous ozone and polar stratospheric cloud observations at South Pole Station during winter and spring 1991, *J. Geophys. Res., 98,* 12,741-12,751, 1993.

Schäfer, P. Scheuch, M. Langer, K. H. Fricke, U. von Zahn, and B. M. Knudsen, Lidar observations of polar stratospheric clouds at Andoya, Norway, in January 1992, *Geophys. Res. Lett., 21,* 1307-1310, 1994.

Schlager, H., F. Arnold, D. Hofmann, and T. Deshler, Balloon observations of nitric acid aerosol formation in the Arctic stratosphere; 1, Gaseous nitric acid, *Geophys. Res. Lett., 17,* 1275-1278, 1990.

Schoeberl, M. R., L. R. Lait, P. A. Newman, and J. E. Rosenfield, The structure of the polar vortex, *J. Geophys. Res., 97,* 1992.

Solomon, S., Progress towards a quantitative understanding of Antarctic ozone depletion, *Nature, 347,* 347-354, 1990.

Steele, H.M., and P. Hamill, Effect of temperature and humidity on the growth and optical properties of sulfuric acid-water droplets in the stratosphere, *J. Aerosol Sci., 12,* 517-528, 1981.

Stormer, C., Remarkable clouds at high altitudes, *Nature, 123,* 260-261, 1929.

Tabazadeh, A., R. P. Turco, K. Drdla, and M. Z. Jacobson, A study of type I polar stratospheric cloud formation, *Geophys. Res. Lett., 21,* 1619-1622, 1994.

Tabazadeh, A., O. B. Toon, and P. Hamill, Freezing behavior of stratospheric sulfate aerosols inferred from trajectory studies, *Geophys. Res. Lett., 22,* 1725-1728, 1995.

Tolbert, M. A., Sulfate aerosols and polar stratospheric cloud formation, *Science, 264,* 527-528, 1994.

Toon, O. B., P. Hamill, R. P. Turco, and J. Pinto, Condensation of HNO_3 and HCl in the winter polar stratospheres, *Geophys. Res. Lett., 13,* 1284-1287, 1986.

Toon, O. B., R. P. Turco, J. Jordan, J. Goodman, and G. Ferry, Physical processes in polar stratospheric ice clouds, *J. Geophys. Res., 94,* 11,359-11,380, 1989.

Toon, O. B., E. V. Browell, S. Kinne, and J. Jordan, An analysis of lidar observations of polar stratospheric clouds, *Geophys. Res. Lett., 17,* 393-396, 1990.

Worsnop, D. R., L. E. Fox, M. S. Zahniser, and S. C. Wofsy, Vapor pressures of solid hydrates of nitric acid: Implications for polar stratospheric clouds, *Science, 259,* 71-74, 1993.

Young, A. T., Revised depolarization correction for atmospheric extinction, *Appl. Opt., 19,* 3427-3428, 1980.

Zhang, R., P. J. Woolridge, and M. J. Molina, Vapor pressure measurements for the $H_2SO_4/HNO_3/H_2O$ and $H_2SO_4/HCl/H_2O$ systems: Incorporation of stratospheric acids into background sulfate aerosols, *J. Phys. Chem., 97,* 8541-8548, 1993.

A. Adriani and G. P. Gobbi, Istituto di Fisica dell'Atmosfera, Consiglio Nazionale delle Ricerche, Via G. Galilei, c.p. 27, 00044 Frascati, RM, Italy.(e-mail: adriani@hp.ifsi.fra.cnr.it, gobbi@hp.ifsi.fra.cnr.it)

T. Deshler, Department of Atmospheric Science, University of Wyoming, Laramie, WY 82071. (deshler@marten.UWYO.EDU)

G. Di Donfrancesco, Ente per le Nuove Tecnologie, l'Energia e l'Ambiente, Centro Ricerche Energia Casaccia, 00060 S.Maria di Galeria, RM, Italy. (didonfra@hp.ifsi.fra.cnr.it)

(Received June 24, 1994; revised June 21, 1995;
accepted June 26, 1995.)